Spring 5-11-2018

Stochastic Modeling of Wireless Energy Transfer with Applications in Wireless Displacement Sensing of Structures

Shaun G. Veilleux
University of Maine, Shaun.Veilleux@maine.edu

STOCHASTIC MODELING OF WIRELESS ENERGY TRANSFER WITH APPLICATIONS IN WIRELESS DISPLACEMENT SENSING OF STRUCTURES

By

Shaun Veilleux

B.S University of Maine, 2016

A THESIS

Submitted in Partial Fulfillment of the

Requirements for the Degree of

Master of Science

(in Electrical Engineering)

The Graduate School

The University of Maine

May 2018

Advisory Committee:

Ali Abedi, Professor of Electrical and Computer Engineering, Advisor

Nuri Emanetoglu, Associate Professor of Electrical and Computer Engineering

Richard Eason, Associate Professor of Electrical and Computer Engineering

STOCHASTIC MODELING OF WIRELESS ENERGY TRANSFER WITH APPLICATIONS IN WIRELESS DISPLACEMENT SENSING OF STRUCTURES

By Shaun Veilleux

Thesis Advisor: Ali Abedi

An Abstract of the Thesis Presented
in Partial Fulfillment of the Requirements for the
Degree of Master of Science
(in Electrical Engineering)
May 2018

Wireless communications are being utilized in nearly every field of work and impact virtually everyone's daily life. With the increased use of wireless sensors, the difficulty of powering them becomes more apparent. One emerging technology is the use of wireless energy transfer which utilizes either a designated transmitter or harvests otherwise wasted energy. Since the amount of transferable wireless energy is limited modeling and simulating a system's probability of operation is desired in order to maximize the run time of the sensor. These simulations allow for the investigation into the impact of a smart scheduling algorithm that can determine the ideal time to transmit a signal and consequently maximize the operational probability.

In addition to the investigations into wireless energy transfer simulations, NASA is interested in using wireless displacement sensor for ground tests of structures such as fuel tanks and other spacecraft components. By converting the data lines from wired to wireless, several miles of cabling per structural test wouldn't need to be installed saving significant time and materials. The designed sensor is to have a

sampling rate of 1-100Hz with a measurable accuracy of at least 3 thousandths of an inch.

A test bed is designed and built to accurately move an armature of a displacement sensor through the operational range in a repeatable fashion. Testing is conducted on an RDP D2/200a linear variable displacement transformer (LVDT) to compare operational performance in both wired and wireless configurations. Test results are presented and conclusions are drawn regarding the possibility of switching existing wired hardware at NASA with equivalent wireless powered units.

Prototypes of the wireless displacement sensor are constructed and tested in the WiSe-Net lab at the University of Maine. In addition the wireless sensor prototype was tested at NASA MSFC to compare the performance to their existing wired displacement sensor system.

ACKNOWLEDGEMENTS

TABLE OF CONTENTS

LIST OF TABLES

LIST OF FIGURES

LIST OF ACRONYMS

AWGN - Additive White Gaussian Noise

COTS - Commercially Of The Shelf

DC - Direct Current

IC - Integrated Circuit

LOS - Line Of Sight

LVDT - Linear Voltage Differential Transformer

MSFC - Marshall Space Flight Center

NASA - National Aeronautics and Space Administration

PCB - Printed Circuit Board

RF - Radio Frequency

WET - Wireless Energy Transfer

Chapter 1
INTRODUCTION

The introduction of cheaper more power efficient sensors has contributed to the growth of data collection seen in all environments including home, automotive, and space exploration. The number of Internet of Things (IoT) devices connected in 2016 was estimated to be 6.1 billion and this number is projected to be as large as 30 billion by the year 2020 [1]. As the number of sensors increases, the complexity required to transmit data and energy effectively increases. As a result the number of wires required to accomplish this task increases which adds weight and increases the required space. Weight becomes a viable issue for aeronautical and space applications. NASA Marshall Space Flight Center estimates that to get a pound of payload to Earth's orbit costs around $10,000 dollars [?]. If the volume and weight of a sensor is reduced, then more sensors can be used to collect more data, more payload can be put into Earth's orbit at a lower cost, or additional other necessary payloads can flown that would otherwise not be possible. Commercial products for transmitting data from a sensor are widely available but a sensor can not be completely wireless unless it also does not require power cables. This can be done with the use of batteries. However, in certain applications the sensor is not easily accessible, making battery replacement a non-viable solution. The feasibility of powering sensors wirelessly with the inclusion of a smart scheduling algorithm is investigated in this thesis. In addition, NASA MSFC is interested in a wireless linear variable displacement transformer (LVDT) sensor that has similar performance to their existing wired solution. The benefits of switching to a standalone wireless system will be the ease and reduced time of the initial setup.

1.1 Background

As the use of wireless data transmission has risen for uses such as WiFi, AM/FM radio, and broadcast TV, the amount of energy on a wireless channel is higher than ever. The majority of this energy goes unused and lost. A company called Powercast Corporation [?] has designed an integrated circuit (IC) that converts a radio frequency (RF) signal into direct current (DC), which allows for power harvesting of this otherwise wasted wireless energy. A field of study that has not been investigated is how to model a system that is using this wireless power harvesting technique. There has, however, been a lot of research into the study of modeling wireless data transfer [2] [3]. This study proposes that it may be possible to use these previously studied models for data transfer and adapt them to model energy transfer. In fact, it may be an easier model because amount of noise, or other wireless signals, on a channel does not impact the performance of a system but rather it may help the system as it increases the available energy. The amount of available wireless power that can be harvested is typically low, on the scale of micro-Watts to milli-Watts [4], which means that any energy that the sensor wastes can be detrimental to the probability it will have enough energy to operate. One aspect of a wireless system that uses a considerable amount of power is the radio transmitter. Even a modern low power radio, such as the NRF52840, will still require 6-13mA at 3.3V to transmit data [5]. In comparison, a low power microcontroller, such as the PIC16F15356, can have a power consumption as low as $32\mu A$ at 1.8V [6] which in nearly 3 orders of magnitude less than the radio.

Since the most power consumption part of a wireless sensor is typically the radio it is desired to not operate the radio under cases where wireless data is likely to be lost. The probability of data being lost can be calculated by measuring the noise on the wireless channel prior to transmitting. If there is a high amount of noise on the wireless channel, then not transmitting at that time is a possibility. Instead of being

transmitted, the data is stored in memory on the microcontroller and transmitted at a later time when the noise is lower and there is a lower probability of transmitting data that could be lost. This leads to the design of a smart scheduling algorithm which can determine when to transmit and when to wait to minimize the probability that a sensor runs out of stored energy.

The second part of this research is the design of a wireless LVDT sensor that will compete with an already existing system that NASA MSFC uses. The LVDT sensor is used to measure the movement of a test object when under an applied force. The existing setup is used with an accuracy of 3 thousandths of an inch and a sample rate that varies from 1 to 100Hz. Additionally, the existing setup requires four wires running from the data acquisition center to the LVDT sensor. On some of the larger test structures, similar to that shown in Figure 1.1, there can be dozens of these sensors that are placed several hundred feet from the data acquisition center.

Figure 1.1: NASA MSFC test structure example.

The result of this setup is that there are over 100 miles of cabling required for a single structural test as seen in the bottom of Figure 1.1. While the pictured

structural test contains over 1000 individual sensors, only a small percentage of them are LVDT sensors. If the standalone wireless LVDT sensor can achieve the same specifications as the wired system then NASA MSFC can investigate changing the remaining sensors to being wireless.

To make the LVDT sensors wireless the system will utilize the same existing LVDT sensors that are in use now. The wireless system will contain the signal conditioning circuitry, a microcontroller, and a radio in a small package so that the system can be remotely placed on the test structure. Then to remotely collect the data, a receiving radio is connected to a storage device, such as a computer, where the data is stored.

1.2   Purpose of Research

Tt is not always possible to run cabling or get physical access to a sensor once it is in its environment. An example for this would be a spacecraft fuel tank, made using a composite material, where cabling would require a hole and access into the tank, which may not be possible for battery replacement. The solution to this issue is to power the sensor using wireless energy transfer. An issue with using this technique is that the amount of transferable energy is relatively low, therefore using an algorithm to maximize the use of the available energy is desired.

NASA MSFC is interested in the wireless LVDT sensor as the setup time for current structural tests can take months, and there can be over a hundred miles of cable that needs to be routed. The wireless LVDT sensor solves this issue as the sensor just needs to be placed on the structure being tested and all the required signal conditioning circuitry and data collection components are integrated with the LVDT sensor. The data is then collected from the sensor using a radio and the data is stored on a remote computer.

1.3   Thesis Organization

The thesis is organized as follows: Chapter 2 describes the theory, simulations, and calculations for the wireless energy transfer and smart scheduling. Chapter 3 presents the design for the wireless LVDT sensor and the required linear test bed for testing the system. Chapter 4 discusses the software required for the wireless LVDT sensor and the linear test bed. Chapter 5 presents the results of the wireless LVDT sensor performance. Chapter 6 concludes the findings and final system performance.

1.4   Summary of Contributions

The first publication contribution covered the design and framework of the stochastic modeling software of wireless energy transfer. The results were published at the following peer reviewed IEEE conference as a short paper.

S. Veilleux, A. Almaghasilah, A. Abedi, and D. Wilkerson, "Stochastic modeling of wireless energy transfer", 2017, *IEEE International Conference on Wireless for Space and Extreme Environments (WiSEE)*, 3 pages, Montreal, QC, Canada, 2017

Analytical models were later designed that covered the calculations to determine expected outages. These calculations are used to assist in deriving a threshold to minimize a system outage. This paper is planned to be submitted as a full paper to another IEEE conference proceeding shortly.

S. Veilleux, K. Bundy, A. Almaghasilah, and A. Abedi, "Transmission Scheduling for Wireless Energy Transfer with Dual Data-Energy Channel Models", 2018, 13 pages, Under Preparation

Chapter 2
WIRELESS ENERGY TRANSFER MODELING

To simulate the probability that a sensor is operational when powered by wireless energy transfer (WET) technology, simulation software in MATLAB is designed. Incoming and outgoing energy in a WET technology system must be modeled using stochastic, opposed to deterministic, models. The simulations are used to estimate how often a wireless sensor will not have enough stored energy to collect and transmit data. If the sensor does not have enough stored energy at a given time then this event is considered an outage. This chapter studies the outage probability bounds with a varying battery size using simulation and analytical methods.

Section 2.1 lists the stochastic wireless channels that are tested under the wireless energy transfer simulations. Section 2.2 proposes a method for modeling the system using a random walk. and Section 2.3 forms analytical expressions to calculated the upper and lower bounds on the outage with a varying battery size.

2.1   Stochastic Wireless Channels

There has been research in the past on the stochastic modeling of a wireless channel, mainly for the use of wireless data transfer [7]. This study investigated the feasibility of adapting them to model wireless energy. Therefore this study will not go into depth on how to find a model for a stochastic channel, but instead investigate how to use existing models. The main models that are used in this study are AWGN [8][9], Rayleigh [10][11], and Rician [12][13] channel models. The uses of these stochastic models can be seen in Table 2.1.

An AWGN stochastic model is suited for point to point communication without the presence of reflections or scattering, and the transmitter and receiver have a direct line of sight (LOS). The amount of energy on an AWGN channel is given by a Gaussian

Table 2.1: Stochastic models and uses.

Model	Definition	Example
AWGN	LOS without fading or reflections	Deep space communication between satellites
Rayleigh	No Dominant signal with fading and reflections	Urban communication with a mobile sensor without LOS
Rician	LOS with fading and reflections	Urban communication with a mobile sensor with LOS

probability density function (PDF) (2.1) and the cumulative density function (CDF) (2.2), which is also known as a normal distribution.

$$Gaussian\_PDF(x|\mu,\sigma) = \frac{1}{\sqrt{2\pi\sigma^2}}e^{-\frac{(x-\mu)^2}{2\sigma^2}} \tag{2.1}$$

$$Gaussian\_CDF(x|\mu,\sigma) = \frac{1}{2}\left[1 + erf\left(\frac{x-\mu}{\sigma\sqrt{2}}\right)\right] \tag{2.2}$$

Where x is a random variable, μ and σ are the mean and variance of the distribution respectively, and erf is the error function which is encountered when the integral of a normal distribution is taken [9]. A Rayleigh stochastic model is used for a channel in which the receiver does not have a dominant received signal, typically due to no LOS, but instead receives reflections of the signal. The transmitting and/or receiving antennas are typically mobile. This results in sections of time that the received power will enter a time of deep fading due to the signals destructively cancel with each other. The Rayleigh channel is given by the Rayleigh PDF (2.3) and the CDF (2.4).

$$Rayleigh\_PDF(x|\sigma) = \frac{x}{\sigma^2}e^{-\frac{x^2}{2\sigma^2}} \tag{2.3}$$

$$Rayleigh\_CDF(x|\sigma) = 1 - e^{\frac{-x^2}{2\sigma^2}} \tag{2.4}$$

where x is a random variable and σ is the scale. A Rician stochastic model is used in similar situations as a Rayleigh model would. There are reflections, scattering and

the antennas can be mobile. The difference is that the Rician model has a dominant signal and typically direct LOS with the transmitter. The Rician channel is given by the Rician PDF (2.5) and the CDF (2.6).

$$Rician\_PDF(x|v,\sigma) = \frac{x}{\sigma^2} e^{-\frac{x^2+v^2}{2\sigma^2}} I_0 \left(\frac{xv}{\sigma^2} \right) \tag{2.5}$$

$$Rician\_CDF(x|v,\sigma) = 1 - Q_1 \left(\frac{v}{\sigma}, \frac{x}{\sigma} \right) \tag{2.6}$$

where x is a random variable, σ and v are the scale and the spacing from the signal respectively, and I_0 is the based off the zeroth order Modified Bessel Function [14] and Q_1 is given by the Marcum Q-function [15]. It should be noticed that the Rician and the Rayleigh CDF are identical if v is equal to zero.

Since there are two wireless transfers used in this system, one for the wireless energy to the sensor and one for the wireless data off of the sensor, two models are required. The outcome of this is that there can be nine different scenarios from the three given stochastic models in Table 2.1. It is required that a stochastic channel is used for the data transfer as there is a variation in power or noise on this channel at any given time. Since this is the case, if there is a high amount of power on the data channel there is a possibility that the data will be lost or corrupted when transmitted. The total amount of power that is available to a wirelessly powered sensor is greatly limited, so any loss in data is not desired as it wastes energy. Therefore, it would be best to not transmit when the chance of losing data is high due to noise levels. Instead, it would be better to wait and transmit the data later when the power on the data channel is lower. Therefore, the designed simulation will take into consideration the amount of noise on a wireless data channel before transmitting data. With this structure setup the basic block diagram of how the simulation software behaves is shown in Figure 2.1.
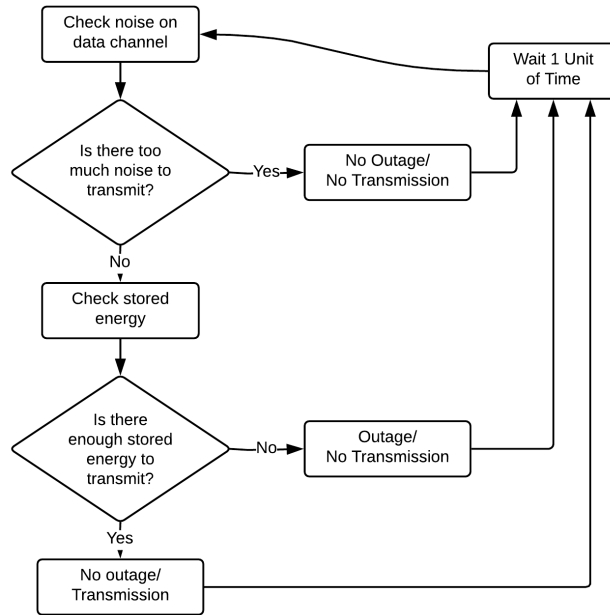
Figure 2.1: Flow chart for designed simulations.

By design, the amount of transmissions and outages are not directly correlated. If there is enough stored energy to transmit, but there is too much noise on the data channel so that the sensor does not transmit, then this is not considered an outage. This was decided to be the case even though the data is not sent because the data can be stored in memory until the next unit of time to transmit if the amount of noise has reduced enough. The result of storing data in memory temporarily is that no data is lost, and as long as the data is not time sensitive this method does not create any issues.

Since a scheduling algorithm is desired to determine what threshold of noise should be tolerated to allow for the greatest amount of transmissions with the least amount of outages, the simulation was run for all nine channel scenarios. The number of transmits versus threshold does not need to be simulated as the number of transmits is proportional to the probability that the amount of noise on the data channel is less than the threshold. This can be calculated by the corresponding CDF functions given above where x is the threshold. To achieve the greatest amount of transmits

the threshold should be as large as possible. This is trivial as the more noise that is tolerated the more often the system will attempt to transmit. However, the amount of outages is not as straight forward. To simulate the probability of outages that a system will have with a set threshold the system needs to be simulated for a very large number of units of time so that the simulated number of outages is close to the mean probability of having an outage. To calculate the percentage of outages that occur in a simulation 2.7 is used.

$$P(outage) = \frac{\# \ of \ times \ stored \ energy \leq 0}{Simulated \ units \ of \ time} \tag{2.7}$$

If the case where each unit of time is independent of each other and at each unit of time the initial stored energy is zero. For each unit of time there is an outage only if the amount of power received is less than the required power to transmit and the amount of noise on the data channel is less than the threshold allows for resulting in the sensor attempting to transmit. If a battery is added to the simulation the total outage decreases since there will be a buffer of energy stored from previous units of time that had received an excess amount of energy. The upper and lower bounds of the system outage are determined in Section 2.3.

2.2   Random Walk Estimation

Since there are two compounded stochastic models that determine if there is a net gain or loss of energy stored at each unit of time it is difficult to determine the resultant model. Additionally, to be able to predict the amount of stored energy after n units of time is nearly impossible without simulating the system. By nature a stochastic model is random with a mean and variance so the two stochastic models can be combined to achieve a single random walk model. This allows for the system

to be modeled with a single mean and variance. The equation for a one dimensional random walk is given as

$$x_n = \mu n + x_0 + \sum_{i=0}^{n} \sigma_i \qquad (2.8)$$

where x_n is the amount of stored energy at the nth unit of time, x_0 is the initial amount of stored energy, μ is the combined mean incoming and outgoing energy, and σ is the variance of the net gain/loss of energy per unit of time. This equation shows that as the system runs indefinitely the variance increases to infinity. Therefore the value of x_n as n approaches infinity can be any value from positive to negative infinity. This is shown by the total variance being equal to

$$VAR_n = \sigma n. \qquad (2.9)$$

While the variance grows linearly with n. The standard deviation grows at a rate of the square root of the variance. For a large time sample of n the mean term in equation 2.8 will increase at a linear rate with respect to n, while the standard deviation grows at a rate of the square root of n. This means that for a large time samples the random walk is nearly equal to

$$x_n \approx \mu n \qquad (2.10)$$

and without a large time sample the expected range of x_n will be is given by

$$x_n = \mu n + x_0 + \sigma n. \qquad (2.11)$$

The result of being able to express the simulation as a random walk is that the amount of energy that is stored at any given time away from the initial starting value can be calculated without calculating the previous time values. Using this method if a sensor has a net loss of energy by design and starts with a charged battery it can

be calculated with a given probability when the sensor will run out of energy and need to be recharged. The same could be done for a net gain of energy. However, if the starting condition is not zero the result will be a sensor that should never be completely discharged.

2.3   Battery Boundary Limits

In section 2.2 the sensors were assumed to have an infinitely sized battery, but in practice this is not the case. Instead the random walk must be bounded. Since the battery size will be limited, then the variance will have a larger impact on the complete number of outages a sensor may experience. Due to the randomness of the simulation it is not trivial to estimate exactly what the outage versus threshold will be for a given battery size. Instead, finding an upper and lower bound on the outage a sensor will experience is possible. A sensor should experience the maximum number of outages when the battery size is as small as possible and the outages will be minimized when the battery size is as large as possible.

The smallest battery possible is to have no battery at all, resulting in a system outage of 100% as the system would not be able to store any energy to transmit at all. This does not give any useful information as a system would never be designed like this. Instead to calculate the upper bound on outages, a system is imagined which has its energy reset to zero after every unit of time. This gives the effect of having no battery between units of time, which creates a memory-less system, but still allows the simulation to operate and result in useful data. The result of this is a system that has an outage only if the amount of noise on the data channel is less than the threshold and the amount of received power is less than that which is required to transmit. So as not to give redundant data the analysis will be performed on a system where the power channel is modeled using an AWGN model and the data channel is modeled using a Rayleigh model. This could be done using any combination of the

12

nine scenarios given in section 2.1 or even a custom power and data channel where the equations are known.

As previously stated the only time that an outage will occur is when the amount of received power is less than that required to transmit and the amount power on the data channel is less the threshold (2.12). The probability that the amount of power on the data channel is less than the set threshold can be calculated using the CDF equation of the data channel (Rayleigh in this scenario) given by (2.4) where x is the set threshold. The probability that the amount of received power is less than that required to transmit can be calculated using the CDF equation of the power channel (AWGN in this scenario) given by (2.2) where x is the required power to transmit. Finally, the probability that both of these occur is the product of the two probabilities since they are mutually exclusive. The resultant equation for the upper bound on outage is given by (2.13) where x_1 is the power required to transmit and x_2 is the set threshold.

$$P(outage) = P(received\_power < transmission\_power) \tag{2.12}$$
$$*P(data\_channel\_noise < threshold)$$

$$P(outage) = \frac{1}{2}\left[1 + erf\left(\frac{x_1 - \mu}{\sigma_1 \sqrt{2}}\right)\right] * \left(1 - e^{\frac{-x_2^2}{2\sigma_2^2}}\right) \tag{2.13}$$

This equation will only hold true when the battery is small enough so that there is no memory between units of time. Once a battery, as a result giving the system memory between units of time, is included then a new method to calculate the lower bound is required. To calculate the lower bound of outages that a system is expected to have the battery is made to be as large as possible. In the case of the simulation the battery has infinite size. As shown in Section 2.2 regardless of the systems power and data channel for a large enough time scale the system follows a random walk where the slope of stored energy is equal to difference of incoming and outgoing power and

the variance can be ignored. Therefore, for the case where an infinite amount of energy can be stored the only time that the system would have an outage is when the mean outgoing energy is larger than the mean incoming energy, thus the system has a net loss of energy on average. If the system had a net gain of energy the system would just continuously gain energy until there is an infinite amount of stored energy giving zero probability of an outage. The slope of the random walk versus threshold and outage versus threshold for a system with an infinitely size battery graphed against each other is shown in Chapter 5, the results section, in Figure 5.4.

To calculate the lower bound the drift versus threshold is taken and for all positive drift values the outage is set to zero. For negative drift values the absolute value of the drift is taken as represented in 2.14

$$LowerBound = \begin{cases} 0 & drift \geq 0 \\ S|drift| & drift \leq 0 \end{cases} \tag{2.14}$$

where drift is the net energy gain or loss and S is a scale value. To calculate the magnitude of the outage to re-scale the drift equation the system must be simulated with a very high threshold so to say that the system transmits 100% of the time. From here there is an analytical expression for the upper and lower bound versus threshold that the outage for a wirelessly powered system can have.

With the upper and lower bound found for a battery of size zero and size infinity to be able to calculate the maximum size battery required to be within a certain range of the minimum outage the random walk algorithm is used. Take, for example, the simulation used for incoming power modeled by an AWGN distribution and the data channel modeled using a Rayleigh distribution. For a given threshold, the easiest case being when the threshold is very large therefore the attempted transmission probability approaches 100%, the mean random walk for stored energy can be modeled using the difference of mean incoming and outgoing energy. If the standard deviation

is added to the mean random walk a range can be found that for any random walk the value will stay within that range x% of the time. For the example of a system being powered by an AWGN distribution for a very high threshold so the data channel model can be ignored it is known that three standard deviations from the mean of a normal distribution 97% of all values fall within this range. If the mean drift is negative and it is known that the mean drift grows faster than the variance, then at some unit of time the mean drift plus three standard deviations there will be a maximum as seen in Figure 5.6. This maximum value is the size the battery must be to ensure that that the outage of the system is within 0.3% of the lower outage bound. Using the three standard deviations rule only works when dealing with a normal distribution. For any other distribution Chebyshev's Inequality [16] must be used which states that

$$P(|X - \mu| \geq k\sigma) \leq \frac{1}{k^2} \tag{2.15}$$

where X is a random variable, μ is the mean expected value, σ^2 is the variance. It can be seen that the probability that a random variable is not within k standard deviations from the mean is equal to $\frac{1}{k^2}$. So for a wide range of distributions the minimum sized battery required for the system outage to fall within 1% of the theoretical lower outage bound a range of 10 standard deviations must be used.

Chapter 3
SYSTEM DESIGN AND TESTING

A proof of concept stand alone wireless LVDT sensor is designed, constructed, and tested. The input to the system is a physical object applying a force that causes linear movement of the LVDT sensors' armature. The output is a wireless transmission of the current position of the sensors' armature. Prototypes of the wireless LVDT sensor are constructed and tested in a lab setting. This chapter describes the design and test of the sensor and the linearly actuated test bed needed to test the sensors performance using a repeatable method.

Section 3.1 lists the specifications for the wireless LVDT sensor. Section 3.2 covers the theory of operation of an LVDT sensor. Section 3.3 describes the design of the LVDT sensor circuit. Section 3.4 describes the design of the linear test bed required to test the wireless LVDT sensor.

3.1   Wireless Sensor Specifications

The primary goal of the wireless LVDT sensor is to prove that a stand alone wireless version of a wired variant, that is currently in use by NASA MSFC, can achieve the same performance. To prevent discrepancies, both the wired and wireless systems would use the same LVDT sensor, a RDP D2/200a. The differences would be in the excitation and signal conditioning/reading circuitry. In addition, the wireless variant would require a radio and the accompanying hardware. Since the wired variant is a commercially off the shelf (COTS) item, the wireless version is designed with the goal to meet or exceed its specifications which are as follows:

- Sampling frequency to be variable between 1-100 Hz

- Transmission distance of up to 25ft

- Total displacement range of at least 0.2 inches

- Resolution of at least 3 thousandths of an inch (0.003 inches)

3.2 LVDT Sensor Operation

The specifications of the wireless LVDT sensor dictate that the displacement range must be at least 0.2 inches, this is dictated by the displacement range of the RDP d2/200a LVDT sensor be used. The operation of an LVDT sensor is different from a linear potentiometer in the sense that an LVDT sensor uses three inductive coils. A main coil, that is driven by an excitation signal, and two sense coils that are wound in opposite directions reference Figure 3.3. The main coil is placed in the center of the two sense coils and there is a floating core with high permeability (typically an iron core) that can slide through the center of all three coils. This causes the excitation signal to leak onto one of the two signal coils or partially split between both coils. This creates a transformer between the coils and since the two signal coils are wound in opposite directions the position of the high permeable core can be detected by the phase and amplitude of the sensed signal. The layout of an LVDT sensor can be seen in Figure 3.1 [17]

In addition to the LVDT sensor seen in Figure 3.1 connected to the core is a rod that extrudes the side of the LVDT sensor. When this rod is moved, in turn moving the core of the LVDT sensor the change in displacement can be detected. Since the physical attributes of the sensor are known the represented schematic diagram can be seen in Figure 3.2.

From the schematic representation it can be seen that if the sensed signal is in phase with the excitation signal, then the core has moved in one direction, and if
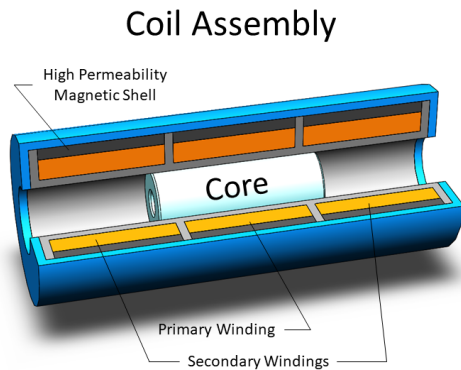
17

Figure 3.1: Physical layout of a LVDT sensor [19].
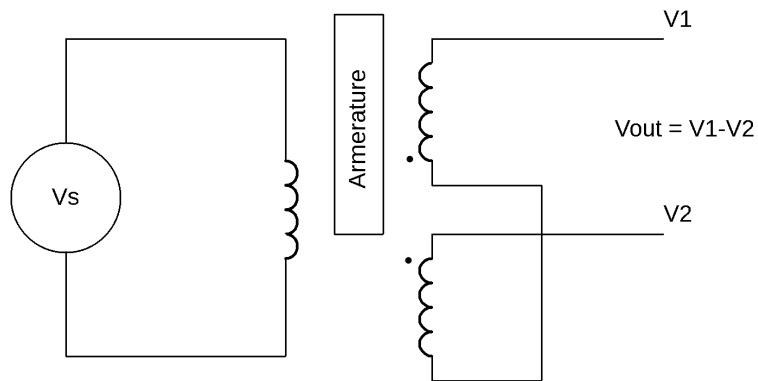
Figure 3.2: Schematic representation of a LVDT sensor.

the sensed signal is 180° out of phase with the excitation signal, then the core has moved in the opposite direction. Additionally, the more the core is positioned in one direction the larger the difference the sense coil voltages will have. This is to say that a larger percentage of the excitation signal will leak onto one of the sense coils in comparison to the other sense coil. To detect the position of the core, the magnitude of the sensed signal determines the absolute position from center and the phase specifies the direction from the center. A signal conditioning circuit using this method with an output voltage versus displacement graph similar to that is displayed in Figure 3.3 [18].

a) Ideal output/displacement curve   b) Exaggerated non−linear curve

Figure 3.3: Output voltage versus displacement [20].
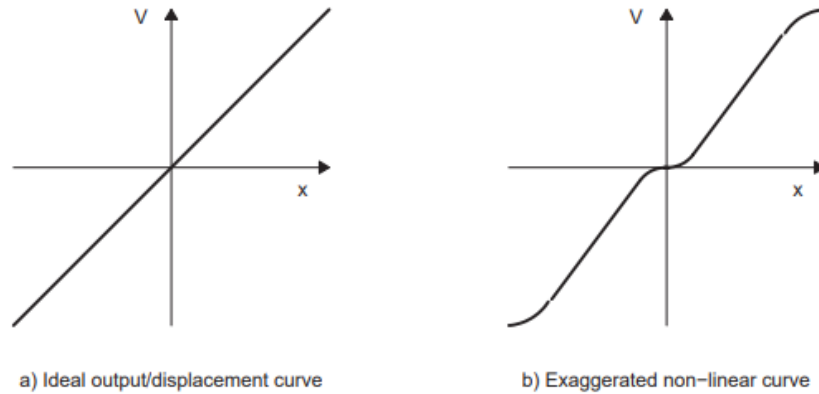
However there are issues inherent to LVDT sensors. The first being that if there is a gap between the main coil and the two sense coils, then there will be a flat spot when crossing the center displacement position. Another issue is that if the windings in each signal coil are not exactly the same, be that the number of windings or placement, the output voltage versus displacement slope on either side of the center displacement position will not be identical. This issue can also occur if the high permeable center core does not have the same dimensions and properties on either end. It is clear that these issues will never be the same between two LVDT sensors and must be characterized before useful data is pulled from the sensors. To be able to characterize each sensor a method of being able to move an LVDT sensors rod linearly at a constant rate and measure the output is required. To be able to achieve this, a linear movement test bed must be designed and built as described in section 3.4.

3.3 Wireless LVDT Sensor Design

In this section the design of the wireless LVDT sensor is discussed. The wireless LVDT sensor is composed of three parts, the LVDT sensor and signal conditioning circuitry, a microcontroller/external ADC, and a wireless transceiver. The LVDT sensor and corresponding signal conditioning circuitry are all contained in a single

package, being the RDP D2/200a which is required to be used as per the specifications set fourth by NASA MSFC. The RDP D2/200a is operated off of a single ended 6 V supply while the remaining components, the microcontroller/ADC and wireless transceiver, require a supply voltage of 3.3V. For this reason the output signal from the LVDT sensor must be conditioned to have a range within 0-3.3 V to ensure that no data is lost due to exceeding the measurable range, and no components are damaged. The completely designed wireless LVDT sensor circuit can be seen in Figure 3.4.
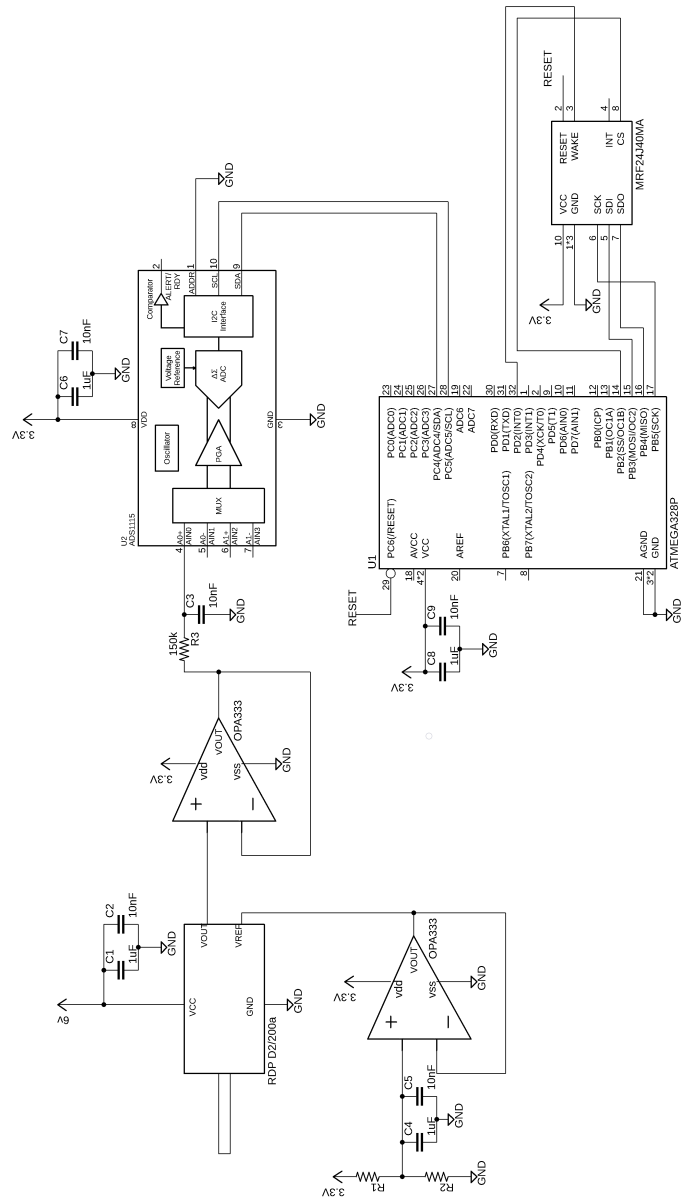

Figure 3.4: Designed wireless LVDT sensor circuit.

The design of the LVDT sensor and signal conditioning circuitry is made easy by using the RDP D2/200a LVDT sensor which contains the circuity required to create the excitation signal and circuitry required to compare the outputs from both sense coils. The output of the RDP D2/200a is a DC signal that varies from a common DC reference signal. Since there is no datasheet or information supplied for the RDP D2/200a sensor by either RDP or NASA MSFC all of the information had to be measured concurrently with the design of the conditioning circuity. The only information available is provided on RDP's website [19] which gave a short excerpt on how an LVDT sensor works and the diagram represented in Figure 3.5.
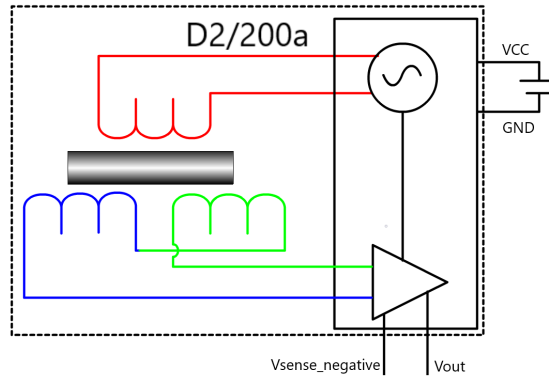
Figure 3.5: RDP D2/200a simple operation diagram [21].

From this operation diagram it can be gathered that the D2/200a is a 4 wire sensor with positive supply, negative supply, positive sense, and negative sense. As given from NASA the sensor is typically operated off of a single 6 V supply. The measured sensor output, V$-out$ with reference to V$_{sense\_negative}$, when the plunger is fully extended is 1.06 V . When the plunger is fully depressed the output voltage is 1.3 V less than V$_{sense\_negative}$. This gives an output voltage range of 2.36 V that is roughly centered around the voltage V$_{sense\_negative}$. This output voltage range is dependent on the supply voltage. Since with the designed 6 V supply the output

range is 2.36V, or less than the 3.3 V that the other components of the system, the output can be fed directly into the microcontroller's external ADC without exceeding the measurement range. To do this $V_{sense\_negative}$ must be set to a value to ensure that the output voltage does not exceed the range of 0-3.3 V on either end. The selected voltage for $V_{sense\_negative}$ is half of 3.3 V or 1.65V. Since the input current for the $V_{sense\_negative}$ port is unknown a simple resistor divider is not used. This is done because if there is current flow then the designed voltage will not be accurate which is necessary to ensure that the output voltage swing remains in the 0-3.3 V range. Instead an op-amp is used in an unity gain buffer configuration, shown in Figure 3.6, which will hold the voltage set by the resistors R1 and R2 even if there is a flow of current into the $V_{sense\_negative}$ port.
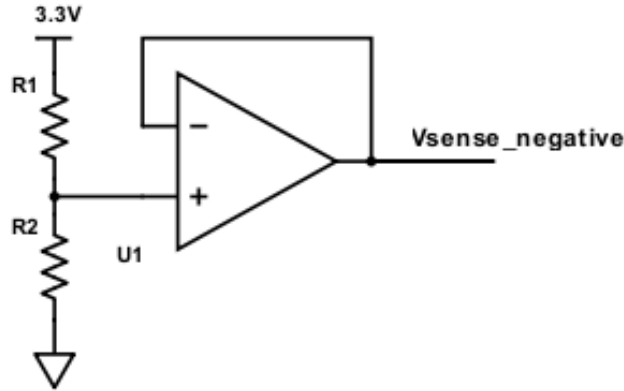
Figure 3.6: Unity Gain buffer op amp for split rail reference voltage.

With this setup $V_{sense\_negative}$ will be equal to

$$V_{sense\_negative} = \frac{R2}{R2 + R1} V_{CC} \tag{3.1}$$

in the case that R1 is equal to R2 then $V_{sense\_negative}$ will be equal to half of V_{CC} or in this case 1.65V. If resistors R1 and R2 are not exactly equal then $V_{sense\_negative}$ will not be exactly 1.65V. As long as the difference is not large enough to cause the

output voltage of the D2/200a sensor to exceed the voltage range of 0-3.3 V then this variation can be removed in software. Using 5% tolerant resistors the maximum range for $V_{sense\_negative}$ to be is 1.56-1.73 V which is not large enough to cause the V_{out} signal to exceed the designed supply voltage range.

The output resistance of the LVDT sensor is also unknown, so to prevent impedance issues a unity gain buffer is used to buffer the output signal before being measured by the ADC. Since a LVDT sensor consists of three inductive coils there is the possibility of voltage spikes so to prevent these and reduce the overall noise, $1\mu F$ and 10nF capacitors are used as bypass capacitors on the positive power supply, $V_{sense\_negative}$, and the output.

To obtain a resolution of 3 thousandths of an inch an ADC with a great enough resolution must be chosen. The D2/200a sensor has a total range of operation of 0.6 inches and the output voltage swing over this range is calculated to be 2.36 V earlier in this section. Using (3.2) the change in voltage the D2/200a sensor outputs for a change in 3 thousands of an inch can be calculated to be 11.8mV.

$$\Delta V = \frac{\Delta d}{R}(V_{tot}) \tag{3.2}$$

where ΔV is the change in voltage, Δd is the change in distance, R is the total measurable range of the LVDT sensor, and V_{tot} is the output voltage range of the LVDT sensor. Using this change in voltage per 3 thousandths of an inch the chosen ADC must be able to detect a change in voltage of at least this small. Since the ADC is operated off of a 3.3 V rail the number of bits the ADC must have is given by (3.3)

$$Required\ bits = \left\lceil log_2\left(\frac{V_{supply}}{\Delta V}\right)\right\rceil \tag{3.3}$$

where ΔV is the change in voltage calculated in (3.2) and V_{supply} is 3.3V. It is calculated that the required number of bits is 8 to be able to have, at least, a resolution of 3 thousandths of an inch. To exceed this the ADS1115 16 bit ADC is chosen to

ensure that the limit of resolution is not due to the ADC. According to the ADS1115 datasheet [18] with an operating range of ± 4.096 V (pg. 17) the LSB resolution is 125μ V which is greater resolution than the 11.8 mV required. The range is selected to be ± 4.096 V even though the supply rails are 0-3.3V, and therefore the full range will not be utilized, because the next lower operating range is ± 2.048 V which is not large enough to cover the full range needed.

Since the chosen ATMEGA328p microprocessor, the ADS1115 external ADC, and the MRF24J40MA wireless transceiver are all contained systems that do not require any external components to operate. The only design work that needed to be done is the connection of the SPI and I2C data lines. In addition 1μF and 10nF bypass capacitors are also used on the supply rails for these components to reduce the measured noise.

3.4 Linear Test Bed Design

In this section a linear movement test bed is designed to help in characterizing non-linearity's of a LVDT sensor and signal conditioning circuit. One of the easiest ways to achieve linear motion without the requirement of manual inputs is the use of a stepper motor paired with a lead screw. Since smaller diameter lead screws are often not straight, the addition of slide rails are required to prevent motion in any direction other than parallel to the LVDT axis of measurement. The linear test bed to be used is designed in SolidWorks and a section view is shown in Figure 3.7.

The test setup consists of an aluminum table which rides on pillow blocks and linear rails that are oriented parallel to the LVDT axis of revolution. Permanently fixed on top of the table is a polymer block which actuates the plunger on the LVDT as the table is moved. The table position is controlled by a lead screw which is attached to a stepper motor with a shaft coupling. The LVDT sensor is then used to measure the movement of this top plate. The stepper motor can easily be driven using
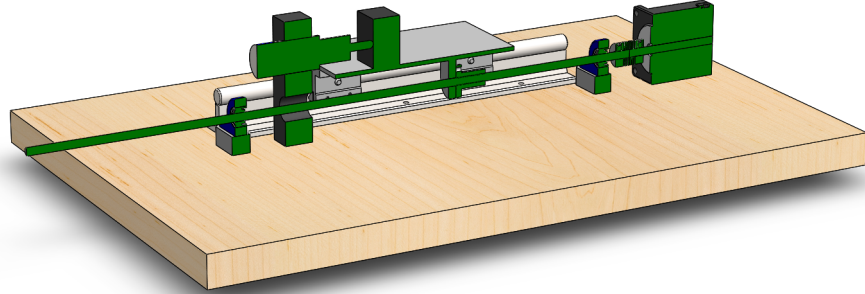
Figure 3.7: Designed linear test bed.

a microcontroller and a stepper motor driver. The chosen driver is the DRV8825, the same microcontroller used to measure samples from the LVDT sensor from the signal conditioning circuit is also used to control the stepper motor. This allows for a sample to be read every step of the stepper motor. The distance that the top plate travels per step can be calculated using

$$\Delta D = \frac{tp}{spr}(threads) \tag{3.4}$$

where ΔD is the change in displacement, spr is the steps per revolution of the stepper motor, tp is the thread pitch of the lead screw, and threads is the number of start threads on the lead screw. In this case the lead screw of the designed test bed has a pitch of 2mm and is a four start lead screw.

The chosen stepper motor has a 1.8° per step and it can be calculated that there are 200 steps per revolution. With this and using (3.4) it can be calculated that the total displacement per step will be 1.57 thousandths of an inch which is less than the LVDT sensor is required to measure accurately. This holds true if the stepper motor driver takes full steps and no micro-stepping is used. If the displacement per step is

25

required to be smaller, micro-stepping can be used. The DRV8825 supports up to a 1/32nd micro-step size which would give a displacement per step of .0492 thousands of an inch. This should not be required though as the wireless LVDT sensor only requires a resolution of 3 thousandths of an inch.

The designed circuit to drive the stepper motor is shown in Figure 3.8 which contains a microcontroller that controls the direction and sends a square wave pulse where every logic change results in a step being taken. The DRV8825 contains the logic and full H-bridge to drive the stepper motor. It is required to have two supply rails going to the IC, a logic supply chosen to be 5V, and a supply to drive the stepper motor chosen to be 24V. These supply rails do not need to share the same ground and can be isolated to prevent noise leaking from the stepper motor logic supply.
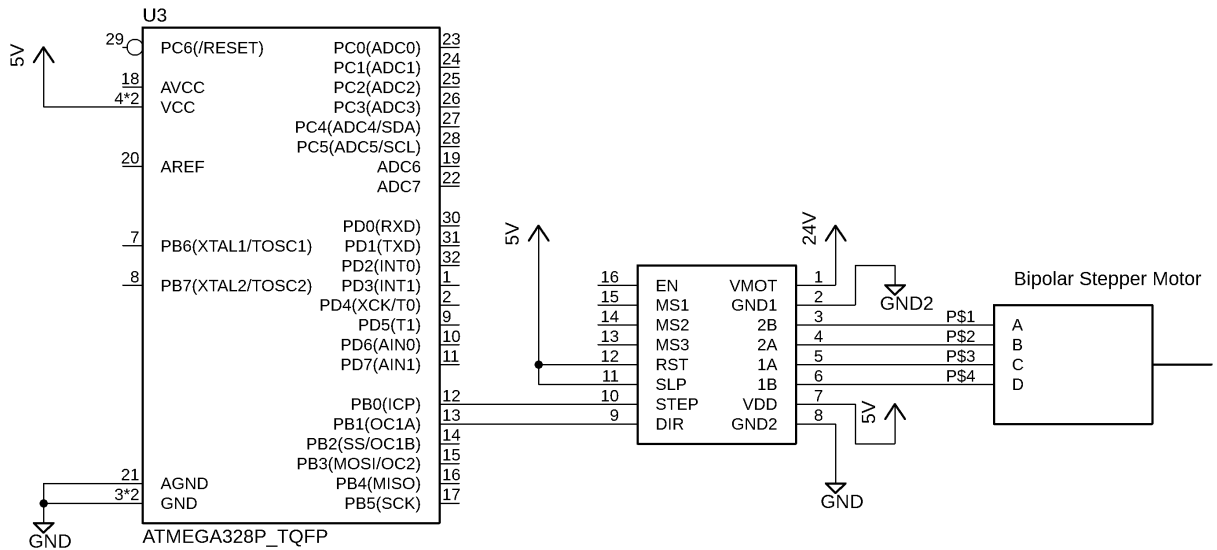

Figure 3.8: Designed test bed motor drive circuit.

Chapter 4
SOFTWARE DESIGN

The proof of concept stand alone wireless LVDT sensor requires software to be able to collect, transmit, and store the data. Section 4.1 covers the design choices of the software in a high level format. Section 4.2 covers the software design for the linear test bed is covered.

4.1   Wireless LVDT Sensor

The wireless LVDT sensor software consists of two sections, data collection and data transmission. The data collection used an external ADS1115 which communicates with the ATMEGA328p microcontroller via I2C. The ADS1115 can have one of four different addresses depending on how the ADDR pin is connected. According to the datasheet [20] the addresses that the ADS1115 can be is shown in Table 4.1. The wireless LVDT sensor is designed to only have a single slave device on the I2C bus so the designed address is to have the ADDR pin connected to ground resulting in the corresponding address of 0x48.

The radio, the MRF24J40MA, communicates with the microcontroller through the SPI bus which requires an additional pin from the microcontroller to drive the chip select (CS) pin of the radio to initiate communication. The way that the radio operates is that it uses the IEEE 802.15.4 PHY packet and MAC frame structure

Table 4.1: ADS1115 Addr pin and slave address.

ADDR Pin Connection	Slave Address
GND	0x48
VDD	0x49
SDA	0x4A
SCL	0x4B

and more specifically for this project the MAC Sublayer Data Frame layout is used. According to the datasheet the layout of the data frame can be seen in Figure 4.1 [21].

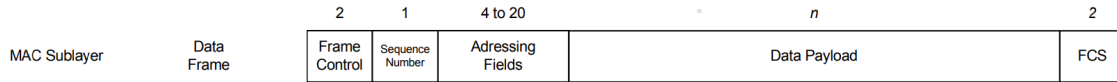|		2	1	4 to 20		n	2
MAC Sublayer	Data Frame	Frame Control	Sequence Number	Adressing Fields		Data Payload	FCS

Figure 4.1: MAC Sublayer data frame layout.

This shows that to transmit n bytes of data there is a required overhead of 10-36 bytes depending on the size of address used. In the case of the wireless LVDT sensor a 2 byte pan and a 2 byte address is utilized resulting in 10 bytes of overhead to transmit n bytes of data. To be able to detect if a packet of data is lost during transmission, the data sent per transmission is the position of the LVDT sensor and a packet count that counted from 1-200. The position of the LVDT sensor required two bytes of data as it was collected from a 16-bit ADC. The packet count was chosen to be 1-200 as all the values can be represented with a single byte of data to keep the transmission packet as small as possible. The result is that each packet is a size of 13 bytes. The library used to control the MRF24J40MA required all the data that is transmitted to be of data type char. This meant that to transmit the position data the 2 bytes of data had to be split into an upper and lower byte and stored into respective chars.

The software of the wireless LVDT sensor follows the block diagram represented in Figure 4.2. To initialize the MRF24J40MA transceiver radio the microcontroller must send the the pan address and the address that the transceiver is to use. The initialization of the ADS1115 consisted of setting the I2C slave address and setting the ADC range, which as calculated in Section 3.3 the range required is ±4.096V which for the ADS1115 is a gain of 1. With the initialization done the system loops indefinitely at a frequency of one over one unit of time. Each iteration a sample from

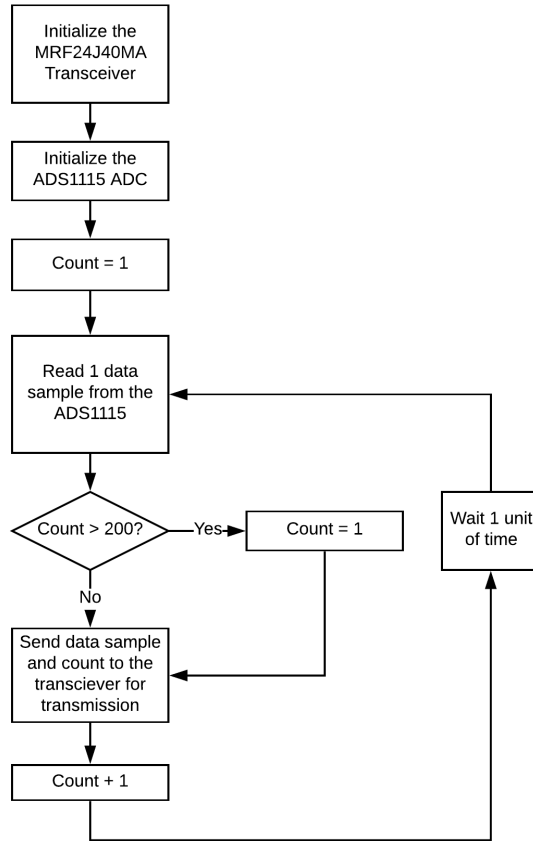the ADS1115 is read and transmitted along with a packet count value which loops through each value from 1-200.

Figure 4.2: Block diagram for wireless LVDT sensor operation.

4.2 Linear Test Bed

The linear test bed is used to test the wireless LVDT sensor using an automated method which can take accurate known step sizes. As designed in Section 3.4 the linear test bed utilizes a DRV8825 stepper motor driver which requires two signals from a microcontroller, a direction signal, and a step signal. The direction signal causes the stepper motor to rotate either clockwise or counter clockwise when a digital high and the opposite direction when a digital low. The step signal causes the stepper motor to take a single step every time it goes from a digital low to a

digital high. Since controlling the linear test bed only requires two digital pins on the microcontroller the same microcontroller can be used to collect data from the LVDT sensor and drive the stepper motor at the same time. This is done to test the performance of LVDT sensor alone without the wireless transceiver.

As calculated in Section 3.4 each step of the stepper motor results in a change in displacement of 1.57 thousands of an inch and it is known that the RDP D2/200a has a sensing range of .6 inches. This gives a total number of steps that the stepper motor can take and remain in range of the RDP D2/200a is 382 steps. To avoid fully depressing the armature of the LVDT sensor and thus damaging it, only 250 steps are used, which is a travel of about .4 inches.
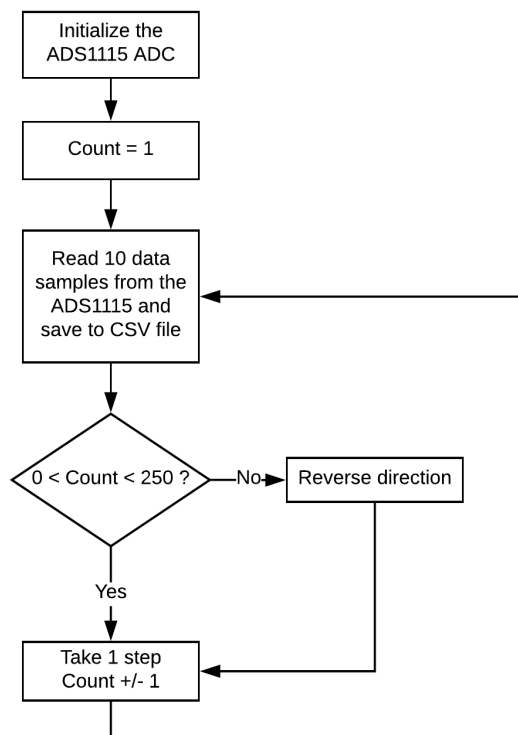

Figure 4.3: Block diagram for linear test bed.

With this design, the block diagram for the code is represented in Figure 4.3. The setup of this test is similar to that of the normal operation for the wireless LVDT

sensor. With the change that instead of transmitting the data wirelessly and just sending it to a computer to be saved to a CSV file. Also instead of the count rolling over from 200 back to 1 instead the count goes from 1 to 250 back to 1. There are 10 samples read at each step of the stepper motor to measure and see if there is substantial noise to change the reading of the LVDT sensor.

Chapter 5
EXPERIMENTAL RESULTS

The prototype of a wireless LVDT displacement sensor was built and tested to meet the specifications and design set fourth and calculated in Chapter 2. Accompanying the wireless LVDT displacement sensor required the construction and testing of a linear test bed as well as performance measurements of the wireless MRF24J40ma transceiver.

The results from the wireless energy transfer simulations are laid out in Section 5.1. Section 5.2 covers the performance of the wireless LVDT sensor and linear test bed. Section 5.3 describes the performance of the first iteration of the wireless LVDT sensor with the wireless transceiver performance as tested at NASA MSFC.

5.1   Wireless Energy Transfer Simulation Results

In Chapter 2 a simulation model was designed along with methods to calculate the upper and lower outage bounds of a system powered by WET. This section will cover the results of the simulation with the example of a system that on average received 1 unit of energy per unit time, the required energy to transmit is 1.1 units of energy, the threshold range is 0-3 units of power on a linear scale, and for each threshold there are 2.5×10^5 units of time simulated. The number of simulated units of time was chosen to be large enough where the results would not vary between simulations. By simulating the system as designed in Section 2.1 and Figure 2.1, the resultant graph for outage versus threshold is given in Figure 5.1. It is noticed that the outage of a network closely resembles that of a CDF function. It is also noticed that the maximum outage is similar for all networks sharing the same power channel and the shape is similar among all networks sharing the same data channel.
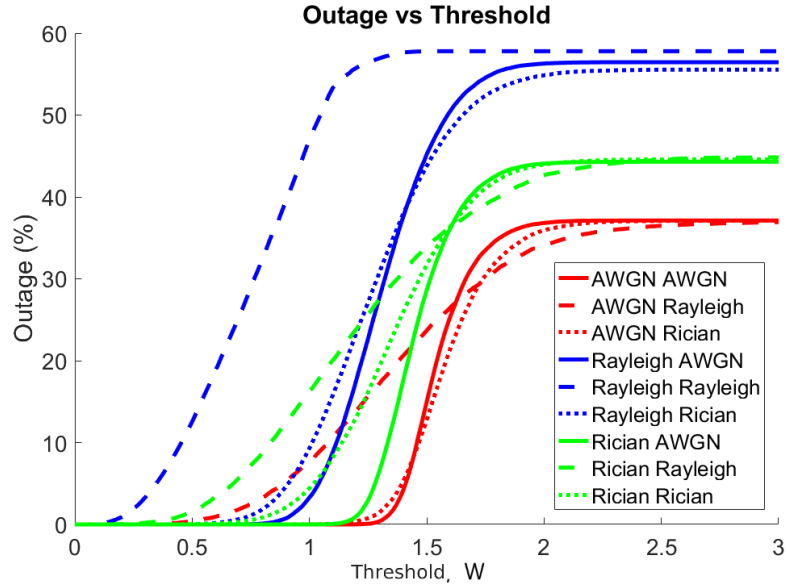
Figure 5.1: Outage vs Threshold for simulated WET.

The outage versus threshold shown in Figure 5.1 was simulated without memory of the amount of stored energy between units of time. This was done to remove the effects of the battery and only investigate the effects of the different power and data channel models. The simulation was run for 2.5×10^5 units of time for each threshold value to collect enough data that the results did not vary between simulations.

As to not give repetitive data the following data is taken in the case where the power channel is modeled by an AWGN model and the data channel is modeled by a Rayleigh model. Simulating the upper bound on outage and comparing it to the upper bound calculation proposed by 2.13 the accuracy of the calculated upper bound can be seen in Figure 5.2. It is seen that the simulated maximum outage and the analytical maximum outage are nearly identical. Since it is not possible to make the battery smaller, when calculating the upper bound, it can be said that this calculated upper bound is the largest expected outage a system will have.
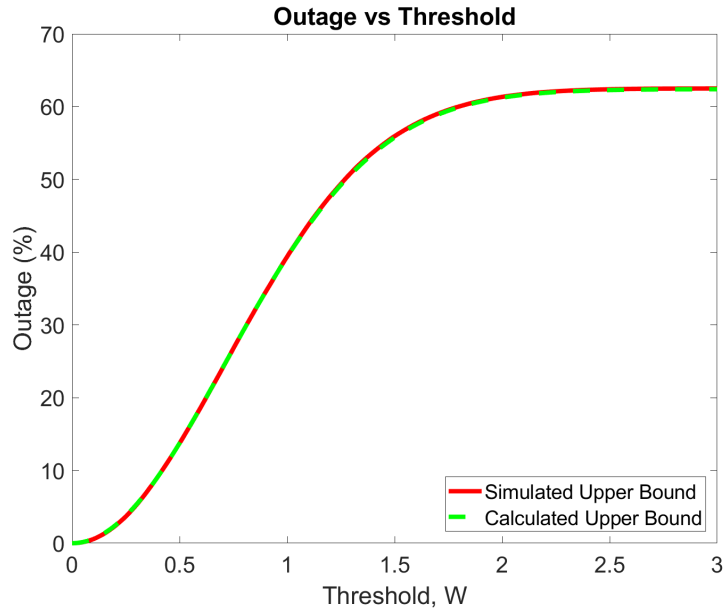
Figure 5.2: Simulated upper bound vs calculated upper bound.

If the size of the battery is increased so energy can be stored between units of time, giving the simulation memory, it can be noticed that the outage is reduced as seen in Figure 5.3.
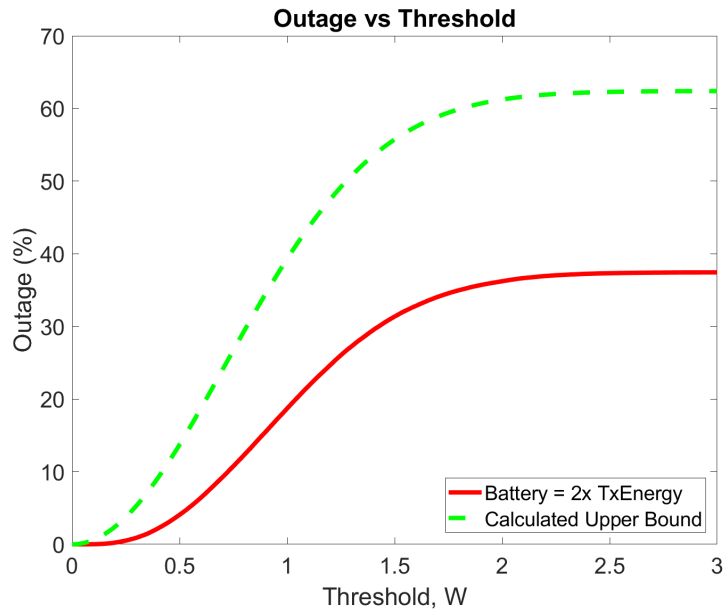

Figure 5.3: Simulated system with battery vs calculated upper bound.

To calculate the lower bound of the system, when the systems battery has infinite size, the net stored energy drift is used. The only time that there is expected to be an outage is when the system on average has a negative net energy gain. This can be seen in Figure 5.4. It should be noticed that if the drift of the net energy gain is positive for a system with an infinitely sized battery there is no outage. Furthermore the shape of the outage lower bound is given by the drift when the drift is negative.
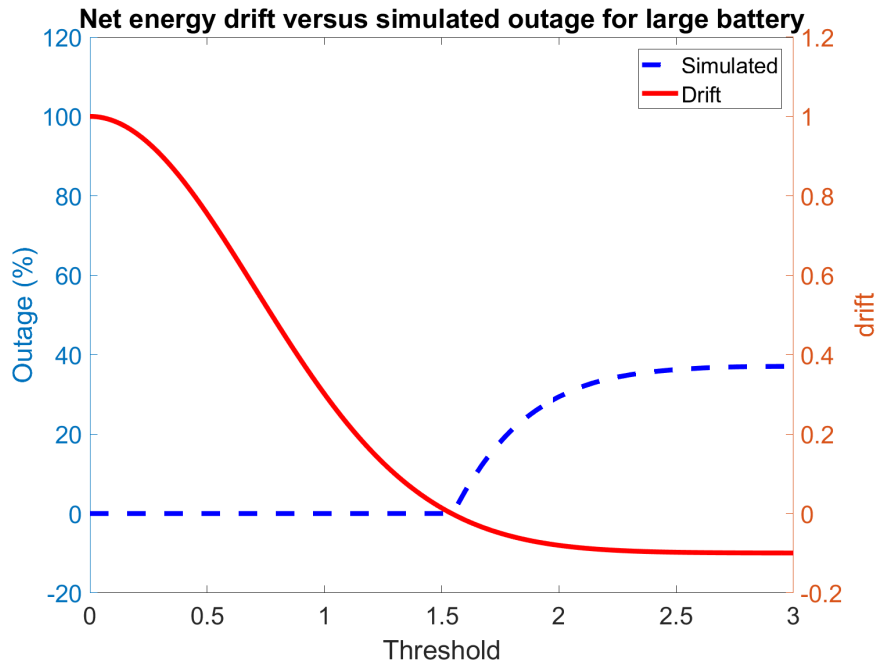

Figure 5.4: Simulated outage with infinitely large battery versus net energy gain.

It should be noted that the actual outage versus threshold line converges the the lower bound quickly as the battery size increases. This can be seen in Figure 5.5. With this a system can be simulated and a threshold can be chosen to achieve a minimum specified outage that is tolerated. Additionally these steps can be used to determine how much power can be used by a system and how often the system can be operational with a given amount of power supplied to it.

With the upper and lower bound found for a battery of size zero and size infinity to be able to calculate the maximum size battery required to be within a certain range of the minimum outage the random walk algorithm is used. Take, for example, the
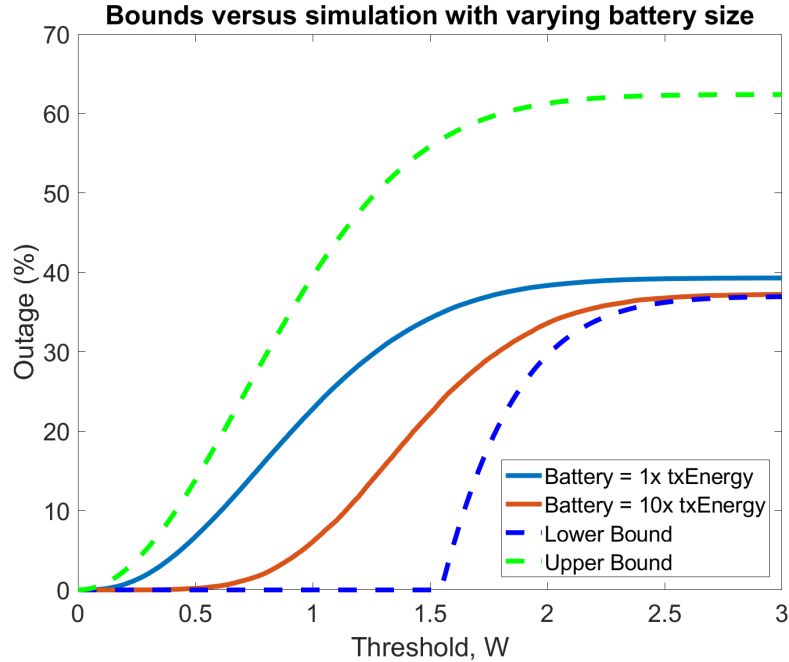
Figure 5.5: Analytically calculated outage bounds versus simulated system with battery size of 1 and 10 times required transmit energy.

simulation used for incoming power modeled by an AWGN distribution and the data channel modeled using a Rayleigh distribution. For a given threshold, the easiest case being when the threshold is very large therefore the attempted transmission probability approaches 100%, the mean random walk for stored energy can be modeled using the difference of mean incoming and outgoing energy. If the standard deviation is added to the mean random walk a range can be found that for any random walk the value will stay within that range x% of the time. For the example of a system being powered by an AWGN distribution for a very high threshold so the data channel model can be ignored it is known that three standard deviations from the mean of a normal distribution 97% of all values fall within this range. When the mean random walk plus three standard deviations are plotted as seen in Figure 5.6 it can be seen that there is peak value.

As shown in plot 5.6 the maximum value is calculated to be 2.2497 at a unit of time of 24 units after starting. Therefore it can be said that for any random walk
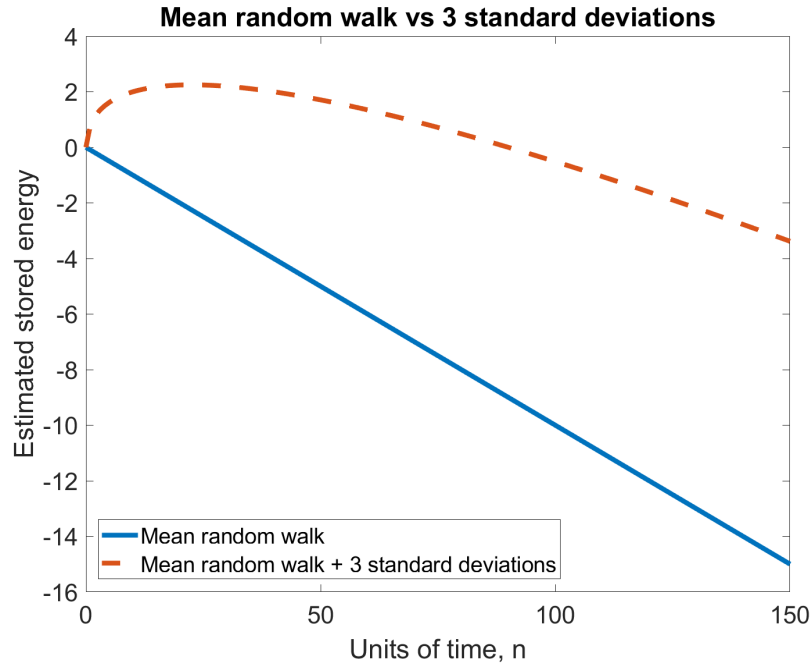
36

Figure 5.6: Mean random walk versus mean random walk plus 3 standard deviations.

there is a 99.7% probability that it will not exceed a stored energy value of 2.2497 in the next unit of time. If the outage of a system with this size battery is plotted against the lower bound calculated in Figure 5.5 it can be seen that the outage for a very high threshold is similar to that of the lower bound. This is shown in Figure 5.7.

It can also be seen that the system outage does not follow the lower bound for any threshold that is not very high. That is because the minimum required battery size is only true for a single threshold and must be recalculated for each desired threshold. To be able to calculate the minimum battery size for a lower threshold the variances for both channels must be combined. This will remove the fact that 99.7% of the values fall within 3 standard deviations from the mean. That is because this rule is only true for purely normal distributions. Instead Chebyshev's Inequality [16] must be used.
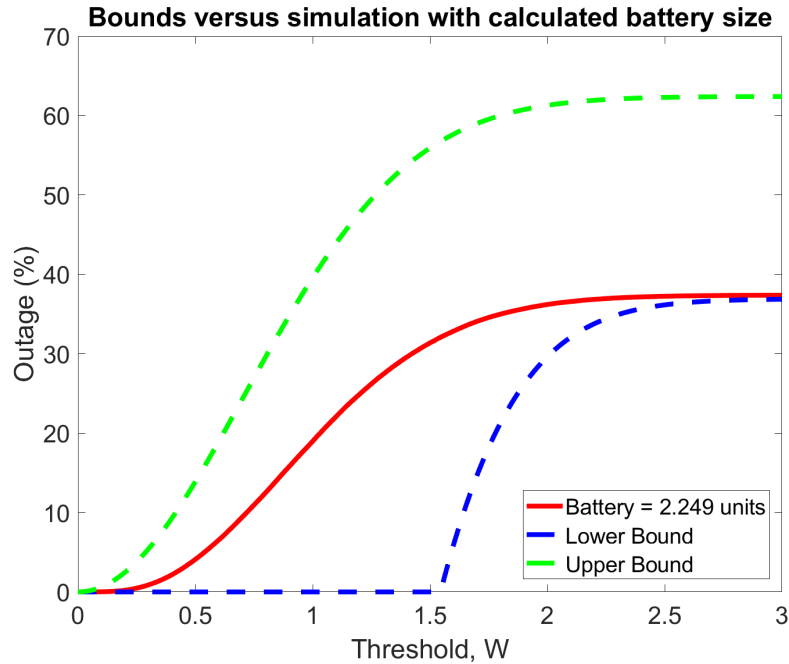
Figure 5.7: Simulated outage of a system with a battery size of 2.2497 versus theoretical bounds.

5.2 LVDT Sensor and Linear Test Bed

To be able to test the accuracy of the designed LVDT displacement sensor a way of moving the armature on the sensor in a predictable and accurate way was necessary. To do this a linear test bed was designed in section 3.4. This section goes over the build, performance, and issues with the linear test bed.

The build of the linear test bed followed the design shown in Figure 3.7 with the change that the base was made from an aluminum plate instead of the shown wooden base. The built linear test bed with the LVDT displacement sensor attached can be seen in Figure 5.8.

The issues with the test bed build are that the bearings used can bind when moving back and forth on the slide rails. The lead screw is not perfectly straight, which can be noticed when the stepper motor is spinning. The plastic hold for the LVDT displacement sensor does not sit perfectly straight due to the mounting holes being drilled at a skewed angle. The bearings and the lead screw issues do not pose
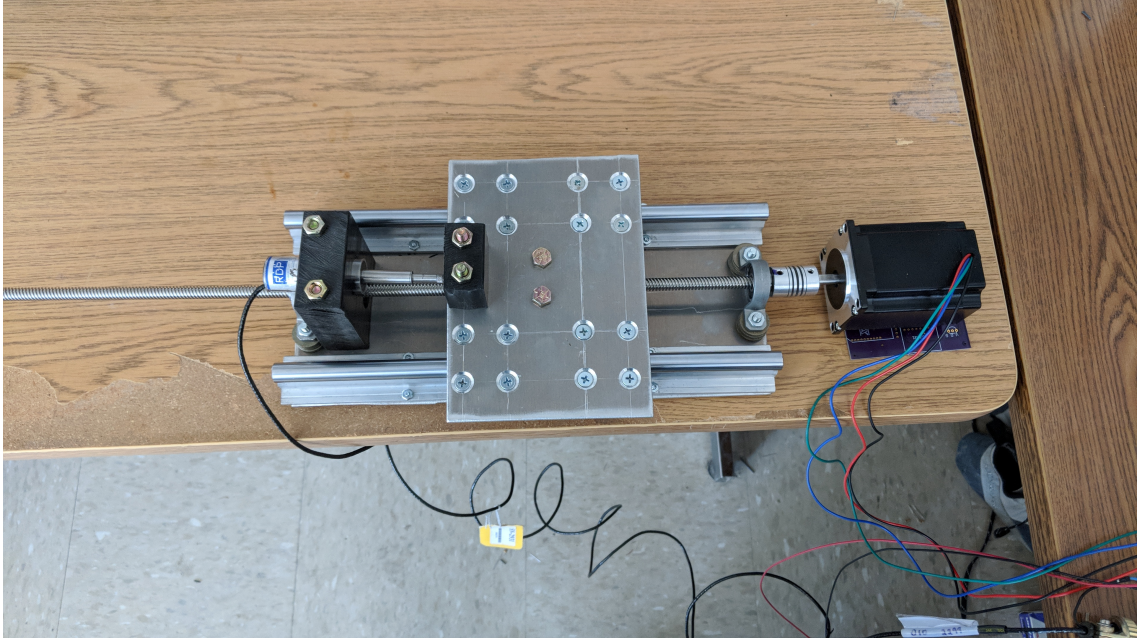
Figure 5.8: Built linear test bed.

an issue due to the fact that the stepper motor has enough torque to overcome the binding of the bearings and the slide rails prevent the sliding plate from moving in any directions other than the desired axis. The holding bracket for the LVDT displacement sensor is acceptable also as the armature always contacts the slide plate throughout the complete range of motion and the being at a slight angle does not introduce any non-linearity's into the movement.

With the linear test bed built and operational, it was used to test the performance of the designed LVDT sensor. As discussed in Section 4.2 the test procedure for the LVDT sensor is to test it under 250 steps where each step is 1.57 thousandths of an inch. At each step there will be 10 data samples read, this is done to measure and see if there is any significant noise that is coming out of the LVDT signal conditioning circuit. If there is significant noise that makes the accuracy of the sensor to be less than the specified 3 thousandths of an inch resolution then the system would need to be redesigned to reduce the amount of noise.

The first test that was run was a single sweep from step 0 to 250. This range equates to about .4 inches total. Using the scale that was calculated in the design section the position of the test bed can be calculated using (5.1)

$$position = (.00157)step \qquad (5.1)$$

where .00157 is the calculated displacement change per step and step is the current step from the start the stepper motor is at. The position that is read from the LVDT sensor can be calculated using (5.2)

$$position = (.000125\frac{.6}{2.36})value \qquad (5.2)$$

where the .000125 comes from the least significant bit of the ADC, the .6 is the total range of the LVDT sensor in inches, 2.36 is the voltage swing the LVDT sensor has when the armature is fully extended versus fully depressed, and value is the value read by ADC which measures the output of the LVDT sensor. By applying the scaling values to the measured data the measured position of the LVDT sensor versus the position of the test bed is shown in Figure 5.9. It is noted that the first value read by the LVDT sensor and the first step of the linear test bed are considered to be zero and all values are relative to this first measured position.

It should be noticed that the calculated scaling results nearly in a one to one relationship from what is measured from the LVDT sensor and what is expected from the linear test bed. It is also seen that there are points throughout the motion that are not exactly linear which can be noticed better when the difference between the measured position from the LVDT sensor and the calculated position of the linear test bed is taken. This can be seen in Figure 5.10.

This non-linearity is not an issue as the measured output position versus actual position can be re-scaled using MATLAB. The issue is that it is not known if this non-linearity is introduced by the LVDT sensor or the linear test bed. As discussed
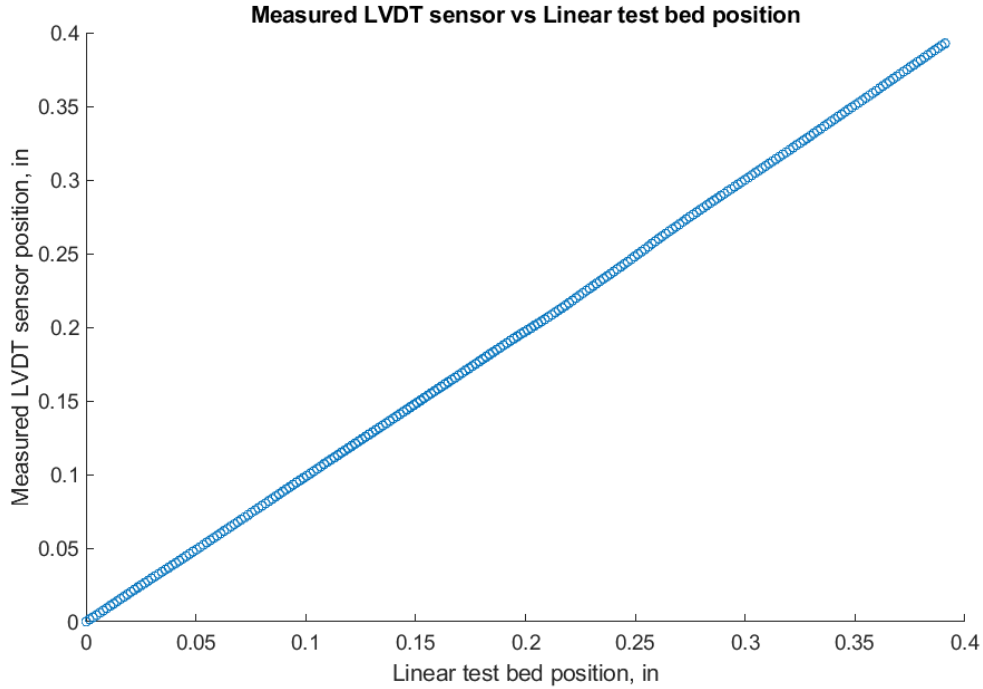
Figure 5.9: Measured LVDT sensor position versus the linear test bed position.

earlier in this section the lead screw used in the linear test bed is not perfectly straight, but slightly bent. While the effects of this are mostly removed by the use of the two slide rails it is possible that this bend still introducing a small amount of non-linearity. The way to determine if this issue is introduced by the linear test bed or the LVDT sensor is to use a system that has a known to be accurate position reading output. This is further discussed in the conclusion section about future work.

What can be seen more importantly from Figure 5.10 is that the amount of measured noise over the 10 samples per step never causes the measured position to vary by more than 3 thousandths of an inch which means that the designed LVDT sensor meets the specification of having a resolution of at least 3 thousandths of an inch. In fact the largest variation in measured position at any step is measured to be 4.76E-4 which is nearly an order of magnitude smaller than specified.
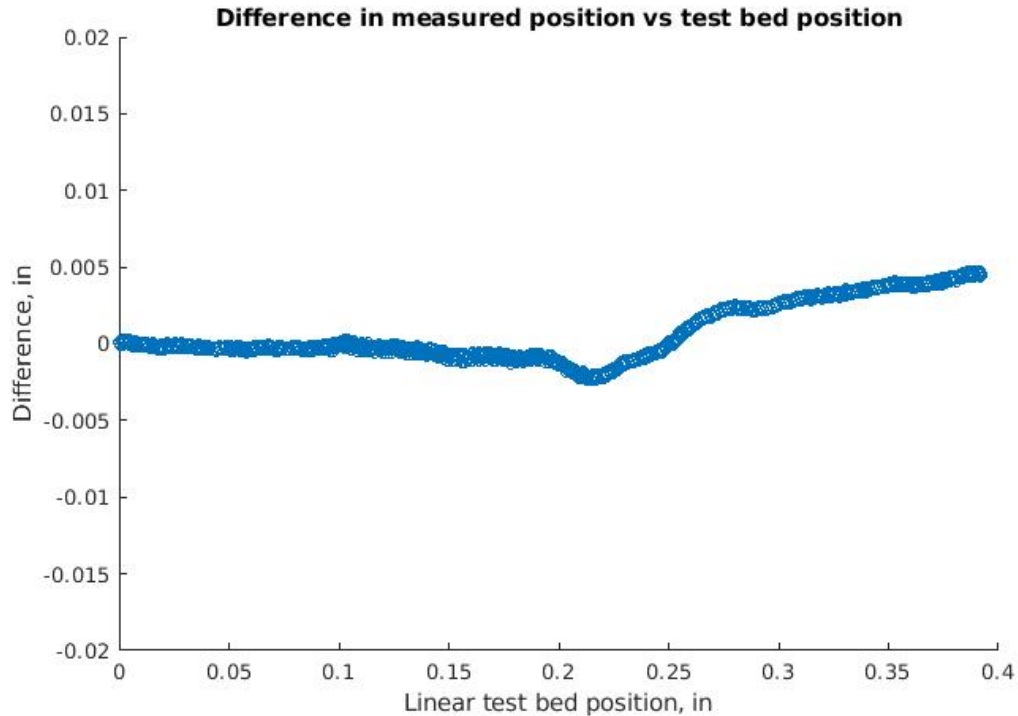
Figure 5.10: Difference in measured position and test bed position.

5.3   NASA Test Results

The first iteration of the designed wireless LVDT displacement sensor utilized a Microstrain LVDT displacement sensor and signal conditioning circuit. This was done so that the main focus could be put on the radios and ensure that they would operate as designed in the structural test environment. The difference between the Microstrain system and the RDP D2/200a and AD698 signal conditioning circuit is that the Microstrain system operates off of 5V, has a 38mm displacement range, and was paired with a 10bit ADC. Since this system was paired with a 10bit ADC and had a larger operating range over a .2 inch test range the best resolution that the system could have would be 1.45 thousandths of an inch. While this does meet the 3 thousandths of an inch specification, it does not allow for any noise on the ADC to be present as any resolution less than 10 bits would result in not meeting the specification. Knowing this limitation, first iteration wireless LVDT displacement sensor was compared to a

wired LVDT displacement sensor utilizing the RDP D2/200a. Since the wired and wireless systems could not by synced properly the wired system was setup to run at 10 times the sample rate compared to the wireless setup, this helped alleviate the syncing issues to some extent.

To ensure that both setups had the same displacement vs time data, both systems were run at the same time and measured the same moving plate. This moving plate was however operated by hand with an analog gauge readout that allowed for precisely moving the plate over a range of $\pm.1$ inches stopping every 25 thousandths of an inch. The first test that was done was with the wireless system sampling at 1 Hz with a transmission distance of 5ft. The output data of both systems compared to each other can be seen in Figure 5.11.
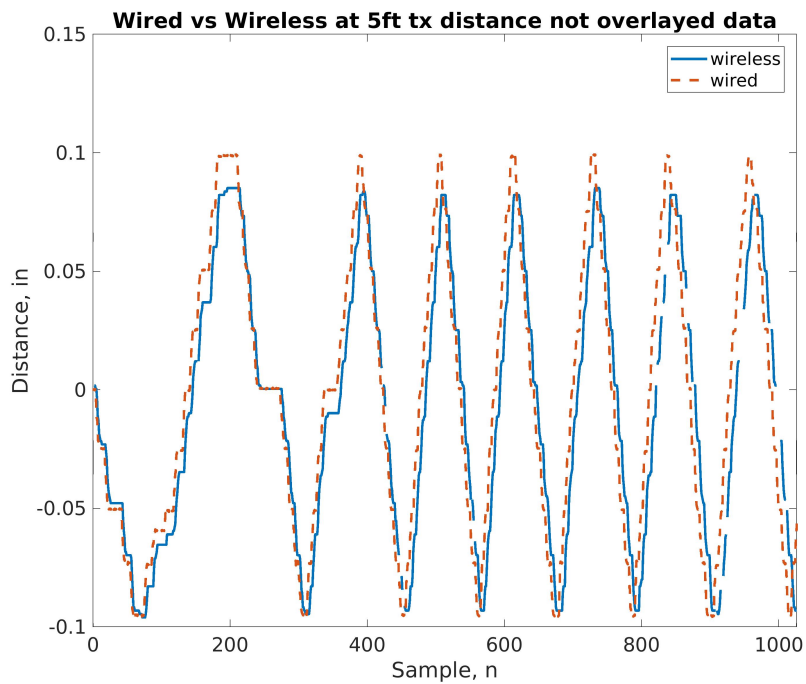

Figure 5.11: Output data for wired and wireless LVDT displacement sensors.

It is seen that the wireless system appears to have a hysteresis issue when moving in the increasing distance direction as seen by the position data lagging behind. This lagging issue is not noticed in when moving in the other direction. This issue is likely

43

due to the Microstrain signal conditioning circuit, and this issue will have to be looked out for on the second iteration of the wireless LVDT displacement sensor. Another noticeable issue is that sampling time between the two systems is not exactly in sync. This is noticed by the position versus sample on the wireless system beginning to lead that of the wired system. To fix this issue the interrupt time calculations need to be redone to ensure that they are correct and if so the addition of an RTC to keep precise time may be required. In addition to testing the precision of the wireless system the packet loss, link quality indicator (LQI), and received signal strength indicator (RSSI) were also measured to test the performance of the radio. The LQI value indicates the quality of the received signal and how well the data can be demodulated, for the radio used in this system the output values range from 0-255 where 0 is very poor LQI and 255 is the best. RSSI does not take into consideration the quality of the received signal but only the amount of power received, for the chosen radio the range is 0-255 where 0 the received signal is below -90dBm and 255 it is greater than -30dBm. At the distance of 5 feet the performance is shown in Figure 5.12

It can be seen that over a distance of 5 ft there were a total of 31 missed packets out of 1026 resulting in a packet loss of 3.02%. It is also noticed that the packets lost often occurred in the same window of time instead of happening completely at random. When compared to the RSSI it can be seen that when the packets were lost the RSSI was also low. When compared to the performance of the radios when the transmission distance is 25 feet it can be seen that there were no lost packets shown in Figure 5.13. This could be because when the radios were at a distance of 5 ft the received signal was too strong that it saturated the receiver, it could also be that the received reflections were also too strong. This is a possibility as a person needed to stand near the transmitter when moving the test slide plate which would introduce reflections. The performance of the LVDT displacement sensor was identical to the performance at 5 ft shown in Figure 5.11.
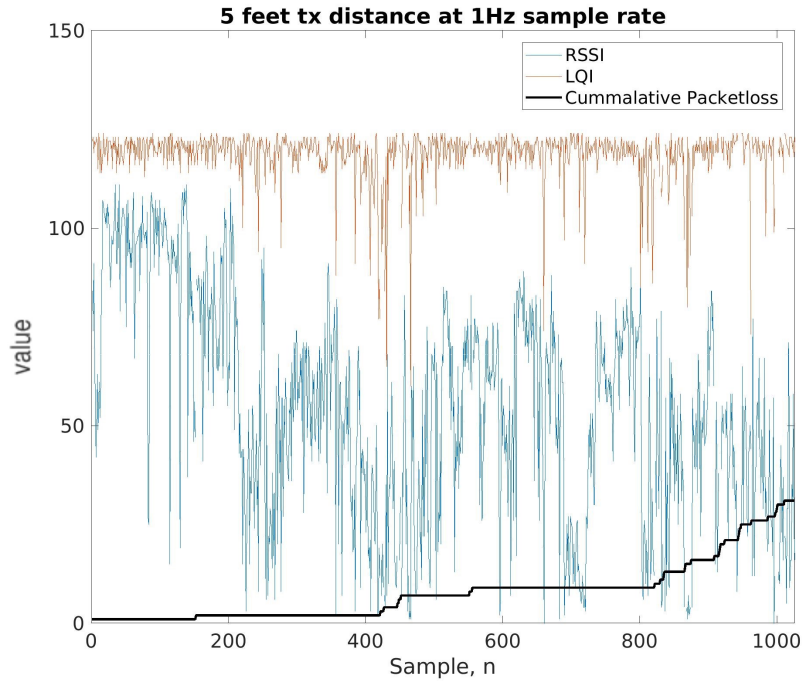
Figure 5.12: Radio performance at 5ft.

It is seen that the change in RSSI and LQI at 25 ft is significantly lower than that at 5ft. The RSSI and LQI data for a sample rate of 100 Hz is similar to that of the 1 Hz sample rate. The RSSI at 5 ft was sporadic which caused many data samples to be lost, while at 100 ft the RSSI was nearly consistent without a large variation. This can be seen in Figure 5.14.

It can be seen that once again the RSSI and LQI at 25 feet were more constant without any major dips. However the packet loss at 25 feet was 2.67%, while the packet loss at 5 feet was only 1.02%. Although the packet loss for the transmission distance of 25 ft was higher, the packet loss only occurred during three time periods while the packet loss was nearly consistent during the entire run time at a transmission distance of 5ft. This packet loss for both runs can be seen in Figure 5.15. This shows the cumulative packet loss divided by the current number of samples taken. With this method the earlier missed packets have a larger impact on the current packet loss percentage. It can be seen that the test at 25 feet had a large spike in packet loss
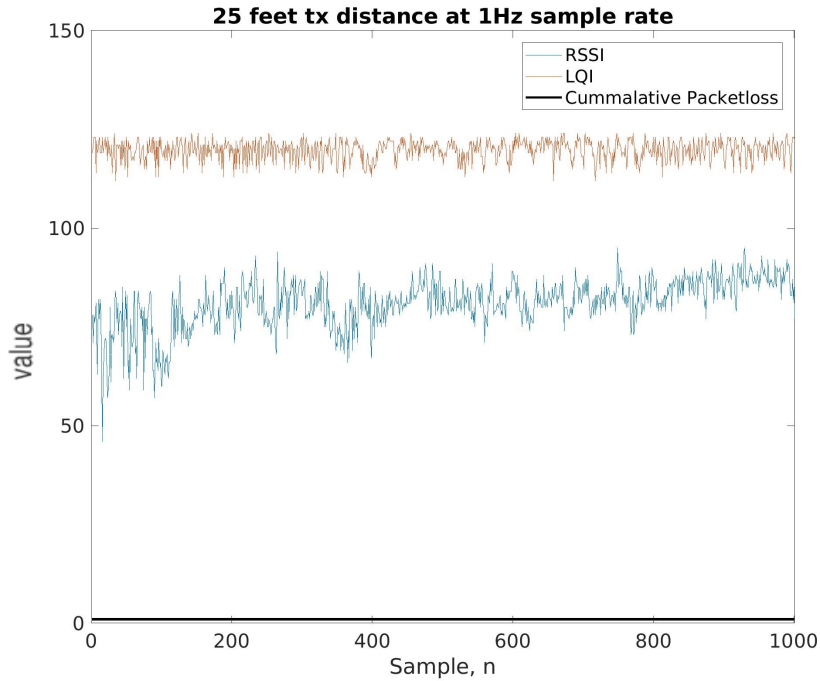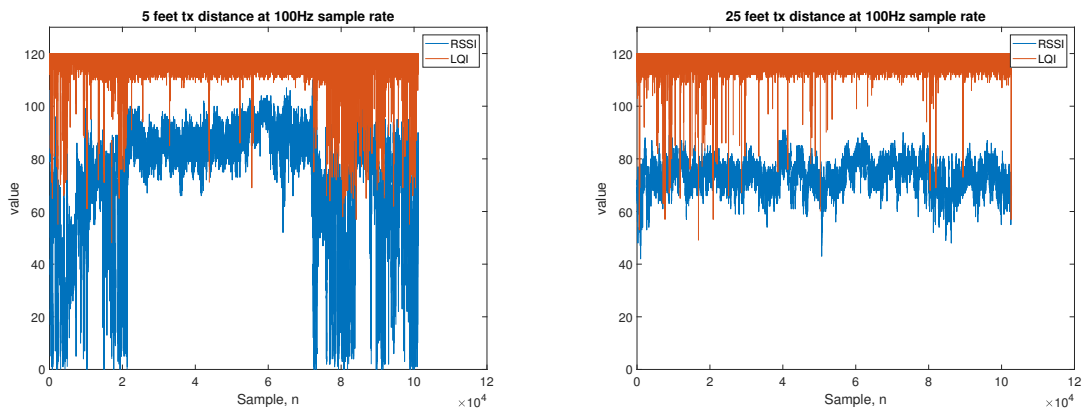
Figure 5.13: Radio performance at 25ft

Figure 5.14: RSSI and LQI with a sample frequency of 100 Hz.

in the beginning and very few after that, therefore it is converging to its final mean packet loss value. The test at 5 feet did not have a section of time that had high packet loss and as a result the cumulative packet loss percentage stays near constant.

The final test that was run was two transmitters that transmitted at 1 Hz. This was done to see if they would interfere with each other and cause more of a packet loss. In Figure 5.16 it can be seen that the packet loss was similar to that of a single
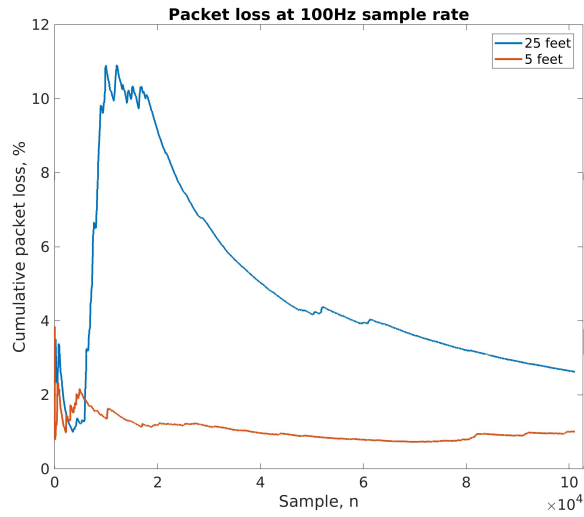
Figure 5.15: Packet loss with sample rate of 100 Hz.

transmitter at 1 Hz at 5 feet away. It should be noted that half way through the test at sample 600 the receiving antenna was moved from a distance of 5 ft away to 25ft. It is also noticed that the majority of the packets lost were at a distance of 25ft. However there is no noticeable distance in the RSSI. Therefore the test would need to be run multiple times and in multiple environments to say if there is any noticeable performance degradation at this distance.
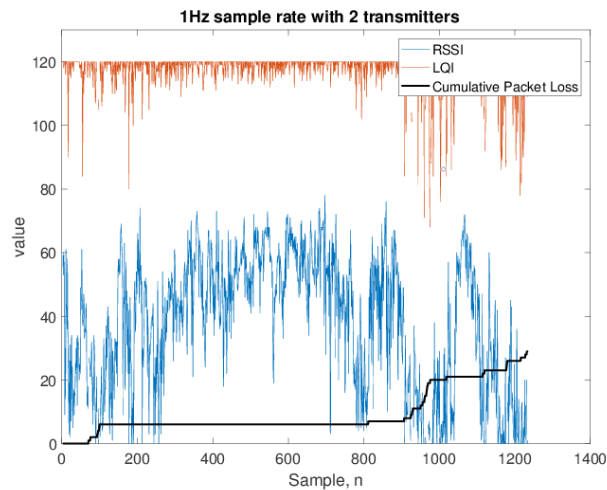

Figure 5.16: Radio performance with two transmitters one receiver.

Chapter 6
CONCLUSIONS

An analysis on modeling a system powered by WET technology has been presented. The use of MATLAB to design simulation software as well as an analytical analysis was performed. It was found that the adaptation of wireless models for data transmission can also be used for wireless energy transfer. From analyzing the simulation results it is found that the outage follows a CDF shape that is a combination of the incoming energy and outgoing CDFs. The lead to the analysis and formulation of methods to calculate the upper and lower outage bounds with the variation of the systems battery size. With the use of a random walk method mathematical methods were formatted to find the bounds. No closed form solution was found to find the magnitude of the lower bound however a method was developed to reduce the number of thresholds required to be simulated down to one. Furthermore a method, that utilized the Chebyshev's inequality, was developed to calculate the required battery size to be within a given range of the lower outage bound.

A wireless LVDT sensor has been designed for the use with an existing LVDT sensor. The specifications were set to meet or exceed that of the already in use wired system at NASA MSFC. The use for the wireless system is to reduce the amount of cabling required in a structural test. This in turn reduces the number of hours it requires to setup each test, resulting in a lower cost. It was found that the wireless system can achieve the same performance as the wired system.

The wireless system was able to achieve a sample rate that could vary from 1Hz to 100Hz and the resolution was measured to be greater than 3 thousandths of an inch. To be able to test the wireless LVDT sensor accurately a linear test bed was needed to be designed and built. By using a stepper motor coupled with a lead screw accurate and repeatable steps, and change in displacement, was possible. One issue

that this caused was any non-linearity's and hysteresis introduced by the linear test bed could not be decoupled from the non-linearity's and hysteresis of the wireless LVDT sensor. To remedy this the system is to be tested at NASA MSFC against their existing wired LVDT sensor system which is known to be accurate.

6.1 Discussion

When this study began the intent was to use wireless energy transfer to power the wireless displacement sensor to allow for an easier setup for the structural tests. However, the Powercast wireless energy transmitter system was tested with a low power wireless sensor that took data readings of the temperature, pressure, and light it received. This sensor required significantly less power than the wireless displacement sensor and even still at a distance between the wireless energy transmitter and the sensor of 5-28 feet it took several seconds to several minutes for enough energy to be collected to take a single data reading. Since the system was specified to be able to transmit the data at a distance of 25 feet if the system required a power transmitter only inches to several feet away then this would negate the benefit of using a wireless energy transmitter as it would still require power cables to be brought nearly all the way to the sensor. For this reason it was decided that the use of wireless energy transfer did not suite the application for powering the wireless displacement sensor.

Another issue that was not foreseen when starting the research was the need to have a test bed to test the wireless displacement sensor. When asked to design the system the specifications were laid out and straight forward to meet however at the University of Maine WiSe-Net lab there was no instrumentation to linearly and predictably actuate the armature of the displacement sensor. This required the design and build of the linear test bed which posed issues of itself as it required machine work to create which the WiSe-Net lab does not have either (as most electronic labs wouldn't). The design was at first designed to be created with a 3D printer but issues

with large flat pieces warping in the past meant that this method would not work well. Access to a machine shop with the required tools was given and the linear test bed was designed with the use of aluminum plates instead of the previously designed 3d printed parts.

The final issue with the linear test bed is that the specifications of it could not be measured on its own. This left the issue of not knowing if the designed wireless displacement sensor has some non-linearity's in it or if they reside in the linear test bed. However for this issue planes have been made to solve it which is discussed in the future work.

6.2   Future Work

The future work for this project will include testing the linear test bed and the finalized wireless LVDT sensor against NASA MSFC's wired LVDT sensor. This is necessary to be able to decouple the issues with testing the linear test bed and wireless LVDT sensor. As of now there are measured hysteresis issues when changing the direction the armature of the LVDT sensor. It is not possible to determine if the issue are due to the circuitry of the LVDT sensor or if the issues reside with the linear test bed. By testing the linear test bed using NASA MSFC's wired LVDT sensor, which is known to give accurate readings, if the same hysteresis issues are witnessed then the issue resides in the linear test bed and not the wireless LVDT sensor.

Beyond testing the designed wireless LVDT sensor and the linear test bed the system needs to have a PCB designed and made as well as an enclosure. This will make the system a more finalized product and less prone to issues as there will be no wires that can be moved.

REFERENCES

[1] A. Nordrum, "Popular internet of things forecast of 50 billion devices by 2020 is outdated," Aug 2016. [Online]. Available: https://spectrum.ieee.org/tech-talk/telecom/internet/popular-internet-of-things-forecast-of-50-billion-devices-by-2020-is-outdated

[2] I. Akbar and W. Tranter, "Order estimation of binary hidden markov wireless channel models in rayleigh fading," *Proceedings 2007 IEEE SoutheastCon*, 2007.

[3] M. Varasteh, B. Rassouli, and B. Clerckx, "Wireless information and power transfer over an awgn channel: Nonlinearity and asymmetric gaussian signaling," *2017 IEEE Information Theory Workshop (ITW)*, 2017.

[4] J. C. Kwan and A. O. Fapojuwo, "Measurement and analysis of available ambient radio frequency energy for wireless energy harvesting," *2016 IEEE 84th Vehicular Technology Conference (VTC-Fall)*, 2016.

[5] *nRF52840 Objective Product Specification v0.5*, Nordic Semiconductor, 12 2016.

[6] *Full-Featured 28/40/44/48-Pin Microcontrollers*, Microchip, 2016.

[7] X. Mao, J. Jin, and J. Yang, "Wireless channel modeling methods: Classification, comparison and application," *2010 5th International Conference on Computer Science Education*, Sep 2010. [Online]. Available: http://ieeexplore.ieee.org/document/5593620/

[8] "comm.awgnchannel." [Online]. Available: https://www.mathworks.com/help/comm/ug/awgn-channel.html

[9] "Normal distribution." [Online]. Available: http://mathworld.wolfram.com/NormalDistribution.html

[10] "Rayleigh distribution." [Online]. Available: http://mathworld.wolfram.com/RayleighDistribution.html

[11] "Rayleigh fading." [Online]. Available: http://www.wirelesscommunication.nl/reference/chaptr03/rayleigh.htm

[12] H. Gudbjartsson and S. Patz, Dec 1995. [Online]. Available: https://www.ncbi.nlm.nih.gov/pmc/articles/PMC2254141/

[13] J. Linnartz, "Distribution of amplitude and power for rician fading." [Online]. Available: http://www.wirelesscommunication.nl/reference/chaptr03/ricepdf/ricepdf.htm

[14] E. W. Weisstein, "Modified bessel function of the first kind." [Online]. Available: http://mathworld.wolfram.com/ModifiedBesselFunctionoftheFirstKind.html

[15] "Rice distribution." [Online]. Available: http://www.mathwave.com/help/easyfit/html/analyses/distributions/rice.html

[16] [Online]. Available: https://www.probabilitycourse.com/chapter6/6_2_2_markov_chebyshev_inequalities.php

[17] "Basics of lvdt," Jul 2017. [Online]. Available: http://www.te.com/usa-en/industries/sensor-solutions/insights/lvdt-tutorial.html

[18] *Signal Conditioning an LVDT Using a TMS320F2812 DSP*, Texas Instruments, 7 2003.

[19] "How it works - dc lvdt." [Online]. Available: http://www.rdpe.com/us/hiw-lvdtdc.htm

[20] *ADS111x Ultra-Small, Low-Power, I2C-Compatible, 860-SPS, 16-Bit ADCs With Internal Reference, Oscillator, and Programmable Comparator*, Texas Instruments, 1 2018.

[21] *MRF24J40 Data Sheet*, Microchip, 2010.
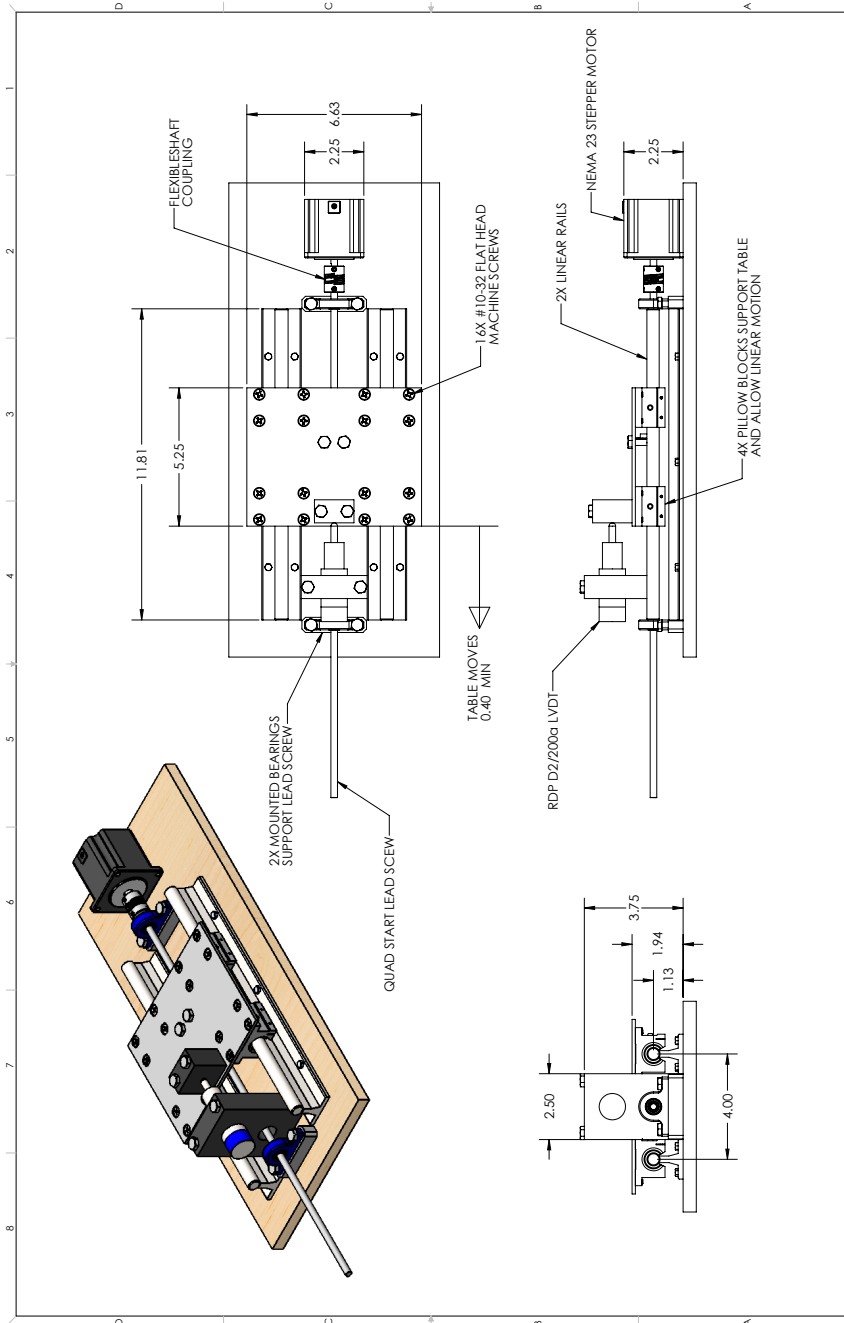
APPENDIX

DIAGRAMS

Figure A.1: Linear test bed diagram.

BIOGRAPHY OF THE AUTHOR

Shaun Veilleux graduated from Messalonskee High School in Oakland, Maine in 2012.

He entered the University of Maine in 2012 and received his Bachelors degree in Electrical Engineering in 2016. In the fall of 2015 he served as a teacher's assistant and continued until the spring of 2017. Starting in the spring of 2017 he began working as a researcher assistant which he continues until the present day. Starting in the fall of 2016 Shaun began his graduate work to his Master's degree which he is expected to receive in May of 2018.

Shaun has accepted a position with Allegro Microsystems as a Product Engineer, starting in Summer 2018. Shaun Veilleux is a candidate for the Master of Science degree in Electrical Engineering from The University of Maine in May 2018.